

RESEARCH ARTICLE

10.1002/2017SW001617

Key Points:

- Solar energetic particle event models with potential for forecasts are needed
- SEPMOD is a model that represents an option, using routinely run ENLIL simulation results
- The model can be applied to any observer location within the ENLIL simulation domain, including planetary sites

Correspondence to:

J. G. Luhmann,
jgluhman@ssl.berkeley.edu

Citation:

Luhmann, J. G., et al. (2017), Modeling solar energetic particle events using ENLIL heliosphere simulations, *Space Weather*, 15, 934–954, doi:10.1002/2017SW001617.







Received 2 MAR 2017

Accepted 17 JUN 2017

Accepted article online 21 JUN 2017

Published online 28 JUL 2017

Modeling solar energetic particle events using ENLIL heliosphere simulations

J. G. Luhmann¹ , M. L. Mays² , D. Odstrcil³, Yan Li¹, H. Bain⁴ , C. O. Lee¹, A. B. Galvin⁵ , R. A. Mewaldt⁶, C. M. S. Cohen⁶ , R. A. Leske⁶, D. Larson¹, and Y. Futaana⁷ 

¹Space Sciences Laboratory, University of California, Berkeley, California, USA, ²CCMC, NASA Goddard Space Flight Center,

³George Mason University, Fairfax, Virginia, USA, ⁴NOAA Space Weather Prediction Center, Boulder, Colorado, USA,

⁵University of New Hampshire, Durham, New Hampshire, USA, ⁶California Institute of Technology, Pasadena, California,

USA, ⁷IRF, Kiruna, Sweden

Abstract Solar energetic particle (SEP) event modeling has gained renewed attention in part because of the availability of a decade of multipoint measurements from STEREO and L1 spacecraft at 1 AU. These observations are coupled with improving simulations of the geometry and strength of heliospheric shocks obtained by using coronagraph images to send erupted material into realistic solar wind backgrounds. The STEREO and ACE measurements in particular have highlighted the sometimes surprisingly widespread nature of SEP events. It is thus an opportune time for testing SEP models, which typically focus on protons ~1–100 MeV, toward both physical insight to these observations and potentially useful space radiation environment forecasting tools. Some approaches emphasize the concept of particle acceleration and propagation from close to the Sun, while others emphasize the local field line connection to a traveling, evolving shock source. Among the latter is the previously introduced SEPMOD treatment, based on the widely accessible and well-exercised WSA-ENLIL-cone model. SEPMOD produces SEP proton time profiles at any location within the ENLIL domain. Here we demonstrate a SEPMOD version that accommodates multiple, concurrent shock sources occurring over periods of several weeks. The results illustrate the importance of considering longer-duration time periods and multiple CME contributions in analyzing, modeling, and forecasting SEP events.

1. Introduction

The ability to understand both the sources of so-called “gradual” 1–100 MeV solar proton events and their variations with space and time has challenged researchers for decades [e.g., Reames, 1999; Mewaldt, 2006; Klecker et al., 2006; Desai and Giacalone, 2016]. These events, the most intense and longest duration solar particle events, can have peak fluxes up to $\sim 10^6$ protons $\text{cm}^{-2} \text{s}^{-1} \text{sr}^{-1} \text{MeV}^{-1}$ and last several days. Cane et al. [1988] first suggested how the observed time profiles of isolated gradual events are spatially organized with respect to the outward-traveling CME-driven interplanetary shock, their likely source. Over the last decade, a new generation of multipoint solar energetic particle (SEP) observations obtained at 1 AU longitudinally separated outposts, by STEREO and ACE, showed that spatially extended events—some even appearing to encircle the Sun—are more common than previously thought [e.g., Richardson et al., 2014]. These observations, together with the ongoing call for SEP event forecasts from space weather information providers [Schrijver et al., 2015], have re-invigorated efforts to model these events on a global heliospheric scale.

Several approaches have been applied toward solar proton event modeling, some building on earlier efforts to interpret simultaneous Helios and IMP spacecraft observations [e.g., Kallenrode, 2003; Reames et al., 2013]. For particles produced close to the Sun, diffusive shock acceleration and transport treatments are generally invoked [e.g., Li et al., 2003, and references therein]. These typically involve numerical solution of a form of the Boltzmann equation developed for describing the propagation of galactic cosmic rays, including magnetic focusing in the diverging heliospheric magnetic field and scattering by small-scale interplanetary field irregularities [e.g., Kota et al., 2005; Kocharov et al., 2009]. With few exceptions, these treatments assume simplified heliospheric conditions and shock geometries to allow use of analytical and/or generalized approximations. The alternative approaches assume a moving, evolving shock source, some based on global, time-dependent descriptions of a heliospheric shock source, and the observer magnetic connection to it along the ambient magnetic field, as the underlying framework [Kallenrode and Wibberenz, 1997; Heras et al., 1992, 1994; Lario et al., 1997, 1998]. Their advantage is the ability to accommodate SEP production over a long radial

baseline, at least up to the observer's location. These treatments generally use back-mapping from the observer along field lines to the modeled shock to determine an empirical source production function based on that shock's properties at the changing field connection point. The resulting SEP time profiles include the prompt component preceding the shock arrival and sometimes the energetic storm particle (ESP) enhancement that accompanies it. Tested source parameters include the shock jumps (compression ratio and velocity) and shock normal angles [e.g., Lario *et al.*, 1998], both of which are important in diffusive shock acceleration theories [e.g., Drury, 1983; Ellison *et al.*, 1990]. Demonstrations of the success of each of these approaches can be seen in the papers describing them including those referenced above, but their use in a regular and even predictive manner remains to be demonstrated. Other recent work toward this goal is described by Aran *et al.* [2006], Schwadron *et al.* [2010], and Marsh *et al.* [2015]. In practice, modeling and forecasting real gradual SEP events require a technique that lends itself to strictly forward modeling based on observations of the solar events that give rise to the shocks.

Early thinking on the matter of SEP event physics [e.g., Palmer, 1982] and even some current interpretations and treatments [e.g., Marsh *et al.*, 2015] that consider an observed SEP time series is dictated by a time profile of injection close to the Sun and subsequent diffusive interplanetary transport. However, several years ago, as part of the Center for Integrated Space Weather Modeling project effort, we developed a model that adopts the alternate perspective where a moving, evolving shock source is the dominant influence [see Luhmann *et al.*, 2004, 2007, 2010]. This was motivated by the earlier work led by Heras and Lario showing that successful simulation of the most important large, gradual events cannot be achieved without taking into account the longer-duration SEP source represented by the traveling interplanetary shock(s) and the changing observer field line connections to it (them). Our SEP event model, SEPMOD, was developed using the heliospheric simulation results from the ENLIL model of Odstrcil *et al.* [2004, 2005]. ENLIL, especially the version incorporating the WSA model of the coronal sources of the solar wind [Arge *et al.*, 2004], is now widely applied in the space weather community. In addition to simulating solar wind structure based on global maps of the observed solar magnetic field, which, via coronal models, describe the coronal hole sources, it includes the so-called "cone model"-initiated interplanetary coronal mass ejections (ICMEs) as an optional addition. These allow introduction of gusts of high-pressure solar wind at ENLIL's inner boundary at $\sim 21 R_s$, whose location, direction, width, and speed are determined from coronagraph images of coronal mass ejections [e.g., see Mays *et al.*, 2015a, and references therein]. The results have been used in retrospective studies, or when based on near real-time observations, for forecasts. WSA-ENLIL-cone models have been subjected to a number of validation studies for both solar wind and shock arrival time predictions [e.g., Taktakishvili *et al.*, 2009; Lee *et al.*, 2013]. At present, they are routinely run at both NOAA's Space Weather Prediction Center (<http://www.swpc.noaa.gov/products/wsa-enlil-solar-wind-prediction>) and the Community Coordinated Modeling Center's Space Weather Research Center (CCMC/SWRC) at NASA Goddard Space Flight Center (<http://ccmc.gsfc.nasa.gov/missionsupport/>).

For applications to SEPMOD, we use specially requested outputs of the WSA-ENLIL-cone model that describe both the heliospheric field lines through a specific observation point as a function of time and the time sequence of shock properties at the observer field line connection point(s) [also see Pomoell *et al.*, 2015, for another example]. These outputs have recently been regularized as part of the product set for ENLIL runs provided by the CCMC [Mays *et al.*, 2015a] and have already been used by Bain *et al.* [2016] to demonstrate that multipoint SEP event time series from STEREO and ACE can be better understood using the observer shock connection information. Note that although subsequent discussions in this paper refer to ENLIL only, it is the combination of WSA, ENLIL, and cone model CMEs that is being applied.

Previous papers on SEPMOD [e.g., Luhmann *et al.*, 2010] described results based on the assumption of only a single shock source at a time in the ENLIL heliospheric simulations. However, it is known from observations from the recent cycle in particular that during active periods, CMEs often occur in spatial and/or temporal clusters. These CMEs can be due to sequential eruptions associated with the same active region but are sometimes from several different coronal sources and locations. It has also been found that the propagation of the resulting ICMEs is affected by the other ICMEs, which may disturb the ambient medium [e.g., Lee *et al.*, 2013]. As a result, it has often been necessary, in modeling specific heliospheric periods, to include all of the significant eruptions detected by the multiperspective imagers. Recent runs of ENLIL now include the option to launch multiple events all around the Sun over time periods of up to weeks. These runs also provide

separate sets of observer-connected field lines and shock parameters for each of the individual ICMEs in the ENLIL run, making it possible to include multiple shock sources in SEP event models like SEPMOD.

Experimentation with the models (ENLIL and SEPMOD) since the previous paper [Luhmann *et al.*, 2010] has led to the practice of using both longer-duration runs (~a solar rotation) and a more distant outer heliospheric boundary (5.3–5.5 AU) to capture SEP event history/context influences. As mentioned above, during active periods in the solar cycle, there are often interplanetary disturbances that overlap, thereby affecting one another. This complication, together with the presence of solar wind stream interaction region compressions in the background solar wind with which the ICMEs interact and sometimes merge [e.g., see *Odstrcil and Pizzo*, 1999], can lead to modified shock propagation (and hence SEP source evolution) and/or magnetic mirroring of SEPs during their transport. Thus, a SEP event model must allow for situations where significant fluxes are traveling back toward the Sun and back out again. Stream interaction regions tend to steepen to a particularly important level beyond 1 AU [e.g., *Pizzo*, 1991], making the orbit of Jupiter a more reasonable outer limit for ENLIL SEPMOD runs than the orbit of Mars at ~1.5 AU.

Here we demonstrate an update of the SEPMOD approach that includes multiple shock sources of SEPs present during the same ENLIL run, within the large heliospheric volume. For this purpose, we use ENLIL simulations covering ~3 weeks when multipoint SEP data were available from STEREO and ACE at ~1 AU, including intervals in August 2010, July 2012, March 2013, April 2013, and January 2014. The first two of these received considerable prior attention [e.g., *Rouillard et al.*, 2011; *Liu et al.*, 2014] because of the strength and/or duration of their activity. In particular, the July 2012 event was considered “Carrington class” because of its extreme parameters as seen at the Sun and in situ at STEREO-A. The August 2010 and July 2012 period observations were also recently subjected to close comparisons of ENLIL shock connection timings with detected SEP event onsets [*Bain et al.*, 2016], providing important background validation for the present SEP event modeling application. The activity in January 2014 was notable because it produced one of only a few ground level events (GLEs) observed on Earth’s surface during solar cycle 24 [*Gopalswamy et al.*, 2015]. We also consider an interval of special interest in March 2015 because it included a period when a significant SEP event was detected by the MAVEN SEP detector in orbit around Mars [*Jakosky et al.*, 2015]. The concluding sections illustrate several applications of SEPMOD ranging from providing context for the near-Mars SEP observations, to Venus aurora interpretive studies, to ground level event source mapping. The results shown here are distinguished from previous demonstrations of SEPMOD described in *Luhmann et al.* [2010] by their more extended time periods and heliocentric radius, and their inclusion of contributions from multiple ENLIL shock sources. They demonstrate the importance, especially at active times, of including both in interpreting SEP observations and generating SEP event models. They also reinforce the notion that regular heliosphere-wide SEP event forecasts can be made today in conjunction with ENLIL runs.

2. SEPMOD Approach

The details of the basic SEPMOD solar energetic particle (SEP) event model were described in two earlier papers [*Luhmann et al.*, 2007, 2010], the latter of which demonstrated its potential use with ENLIL as an interpretive tool for STEREO multipoint SEP events. It was also applied in a preliminary study of the August 2010 period included here [*Luhmann et al.*, 2012], where an option to include a Sun-fixed additional solar flare source (e.g., as suggested by the *Cane et al.* [2006] study) was demonstrated. Briefly, the SEPMOD approach is a compact numerical model incorporating the basic physical concepts of real SEP events—toward both realizing a first approximation to a generalized forward model and evaluating what aspects exert the main control over observed events. SEPMOD’s underlying philosophy, like those of its predecessors mentioned earlier, is that observed SEP flux time profiles—at least in the inner heliosphere—are controlled mainly by changing observer magnetic field connections to a moving, evolving shock source. As part of its present baseline version, it minimizes the influences of diffusive transport and cross-field drifts. The main SEPMOD procedure time-integrates a series of SEP injections from the locations of the shocks on sequential observer-connected interplanetary field lines. This requires a model “data set” of observer field line files from the ENLIL simulation sampled at ~5 min intervals, which include MHD quantities along the field line. ENLIL also produces a separate connected shock file for each observer, with information describing the connected shock parameters at each time step including density, velocity and magnetic field jumps, and shock normal angle. While only one set of observer field line files is required for each ENLIL run, separate observer shock

parameter files are created for each CME-initiated shock in the time period covered. Details on how the shock parameters are derived from the ENLIL simulations are described in *Bain et al.* [2016].

At each time step, SEP MOD injects and then follows a representative set of test particles, typically assumed to be protons, along the observer-connected field line for a nominal number of time steps using a constant energy, guiding center approximation. The latter simply presumes that the guiding center of a particle's motion follows a field line, while focusing and/or mirroring alter(s) its pitch angle in response to the changing magnetic field strength to maintain the first adiabatic invariant $(1 - \mu^2)/B$ (where μ is the cosine of the pitch angle and B the local field magnitude.). Thus, a particle can be focused by the field as it moves outward or mirrored if it moves inward or into field compressions produced by background solar wind structure and/or other ICMEs. Although these assumptions are better suited to the >10 MeV proton energy range, the 1–100 MeV range is nominally included for evaluation purposes. The presently assumed isotropic injections at the point where the observer field line connects to the shock consist of 100 particles at each energy, weighted using functions describing the injected flux and particle energy spectrum based on the ENLIL shock properties (density and velocity jumps). The initial energy spectrum is a power law $KE^{-\gamma}$ where E is the particle energy and the power law index γ is given by $\gamma = 0.5(d + 2)/(d - 1)$ with d equal to the shock compression ratio. This power law formula arises from theoretical treatments of diffusive shock acceleration [e.g., see *Ellison et al.*, 1990, their equation 1]. The particle flux is set by a scaling factor K , which takes into account an empirical result from *Lario et al.* [1998], who found that the log of the inferred production rate is roughly proportional to the shock velocity jump (see section 5.2 of their paper). We use the same value of K for all energies in the present version of SEP MOD, with its nominal value determined from SEP data comparisons, and its variation from case to case caused only by the different ENLIL shock velocity jump histories. A $1/r^2$ factor is added to the injection weighting to account for the spherical expansion of the volume represented by the field line.

If the observer is located within a few tenths of an AU of the shock source and the shock is moving at greater than 300 km/s, an energy-dependent (softer spectrum) ESP flux enhancement is applied that increases as the shock is approached. It is often considered that the ESP part of a SEP event represents an observer's encounter with the shock acceleration region itself [e.g., see *Cohen*, 2006]. As a strawman initial approximation, the ESP flux enhancement in SEP MOD is implemented by adding an additional component to the nominal SEP MOD flux that has an ad hoc spectral index (γ) reduced by -2.5 from the nominal source spectrum. Its contribution is assumed to have a peak value of $50\times$ the nominal model flux, which falls off with distance from the shock location within a layer of half-width 0.1 AU. This approximate manner of accommodating an ESP component results from surveying the literature on the subject [e.g., *Cohen*, 2006; *Mäkelä et al.*, 2011, and references therein] which suggests the range of its observed properties, which seem to depend only roughly on local shock parameters (although stronger shocks are most likely to exhibit ESP enhancements and quasiperpendicular shock related cases sometimes show narrowly confined spike-like flux increases). SEP MOD can be used with or without this ESP enhancement option. It is included in the results shown below, where it affects the SEP fluxes and spectra mainly around the observer shock crossings, having generally modest effects on the overall time series. The use of shock normal angle (θ_{BN}) derived from ENLIL as an additional factor in describing both the injections and the ESP component [e.g., *Tylka and Lee*, 2006, suggest how it may matter] is under evaluation. Similarly, pitch angle scattering around the shock location could be added in Monte Carlo fashion to simulate a more physics-based ESP enhancement.

By time-integrating the fluxes injected at each shock, from the point of each field line shock contact to the observer's location, SEP MOD builds an observer's SEP time profile dominated by the most recent injections. (See the earlier *Luhmann et al.* [2007, 2010] papers for further discussion.) Because of the test particle nature of SEP MOD, individual test particle behavior can be examined. Particles leaving the 5.5 AU outer boundary of the ENLIL domain are presumed lost. Magnetic mirroring occurs during the integration of some SEP trajectories, proceeding for a fixed number of iterations before the calculation moves on to the next observer field line. For newly injected particles traveling inward, a single mirroring closer to the Sun turns most trajectories around, delaying their direct arrival times at the observer. A few particles may pass through the inner ENLIL boundary at $21.5 R_{\odot}$, where they are presumed lost. The effect is that the SEPs from a single injection are spread out in time simply due to their velocities and pitch angle dispersion along the observer field line.

The SEP MOD approach can also be regarded as a test of ENLIL's ability to produce a realistic description of interplanetary shocks, and the field connections to them, throughout the inner heliosphere. SEP MOD results are totally dependent on these features because an observer shock source magnetic field connection is necessary to "observe" the SEPs. The shock remains an evolving source from the time it originates on or first connects to the observer field line to when it disconnects or the shock leaves the ENLIL simulation domain. Other assumptions implicit in the SEP MOD approach are that the particles mainly propagate parallel to the magnetic field, thus implying that perpendicular diffusive propagation and drifts can be neglected to a first approximation (at least in the inner heliosphere). (For an alternate viewpoint on this subject, see *Marsh et al.* [2015]). The current model also tests the ability to reproduce observed SEP events without including the coronal portion of the shock source inside the $\sim 21.5 R_s$ ENLIL inner boundary. (The consequences of this gap, which in principle can eventually be filled-in by an additional model, are revisited in a later section of this paper.)

In earlier applications, SEP MOD worked with only the strongest ENLIL shock connected to the observer at each time step. In this updated version, SEP MOD makes use of shock files produced for each CME in the ENLIL run. SEP MOD is then run for each shock file, producing a separate SEP event time history for each ICME that has a shock connection to the observer. These independent CME-related SEP events are then added to obtain an overall event-integrated SEP time profile. As previously mentioned, in these calculations, the SEPs from one CME shock are affected by the presence of the other CMEs only through the latter's effects on the heliospheric fields experienced along their ENLIL field line trajectories. Thus, the SEPs from one CME-caused shock may mirror or reflect due to the presence of another, or be deviated in their paths from what they would have been in otherwise undisturbed solar wind. The SEPs from an earlier event do not form a "seed" population for other shocks to re-accelerate but contribute to the integrated SEP flux profile. This does not preclude the future addition of other (e.g., re-acceleration) effects in SEP MOD but allows evaluation of the impact of neglecting them—and assuming all of the important energization occurs at the original parent shock(s).

The recent study by *Bain et al.* [2016] of the SEPs seen on STEREO at two locations and ACE at L1 during 1–21 August 2010 and 7–27 July 2012 determined how well ENLIL shock connection timings matched the observed SEP event onsets and durations in those cases. For perspective, it should be mentioned that the earlier study by *Rouillard et al.* [2011] used ENLIL field line back-mapping to test SEP onset timing compared to inferred observer field connection to an EUV wavefront observed in the corona. Although SEP MOD can by design use observer field lines and observer-connected shock data all the way to the solar surface, it is currently limited by the ENLIL model inner boundary at $\sim 21.5 R_s$. For the *Bain et al.* [2016] study, the ENLIL simulation CMEs were adjusted to be especially consistent with both the multiple perspective coronagraph images and the in situ observations of the solar wind and timing of interplanetary shock arrivals detected at the separated spacecraft. Additional adjustments to the CME directions, speeds, and widths were made to capture other shocks—not detected in situ at 1 AU—that had remote connections to the observers along ENLIL field lines according to the SEP observations. Similar retrospectively adjusted (e.g., for additional CMEs and/or improved inferences of their properties) ENLIL runs were used to produce the sequences of observer connected field lines and connected shock properties used in the SEP MOD code results shown here. Readers interested in the considerations that go into cone model parameter determinations and the effects of ambient conditions can find further information in the references in *Mays et al.* [2015a] and *Lee et al.* [2013]. Because SEP MOD results rely so heavily on the heliospheric description used, including the shocks, the importance of this separate modeling task to its successful application cannot be overstated.

3. Results

3.1. Event Period ENLIL Results

Figures 1a–1f show snapshots from the ENLIL runs made for the present study, including an ecliptic plane color contour plot of the plasma velocity on the left, and some observed and modeled time series of the velocity at several observer locations on the right. Although the outer boundary of all of these runs is 5.3–5.5 AU, the results are only shown out to the orbit of Mars in order to emphasize inner heliospheric field and shock geometries. These runs generally involve a setup phase where the undisturbed solar wind is established before the cone model CMEs start. The selected times illustrate some of the disturbances initiated by one

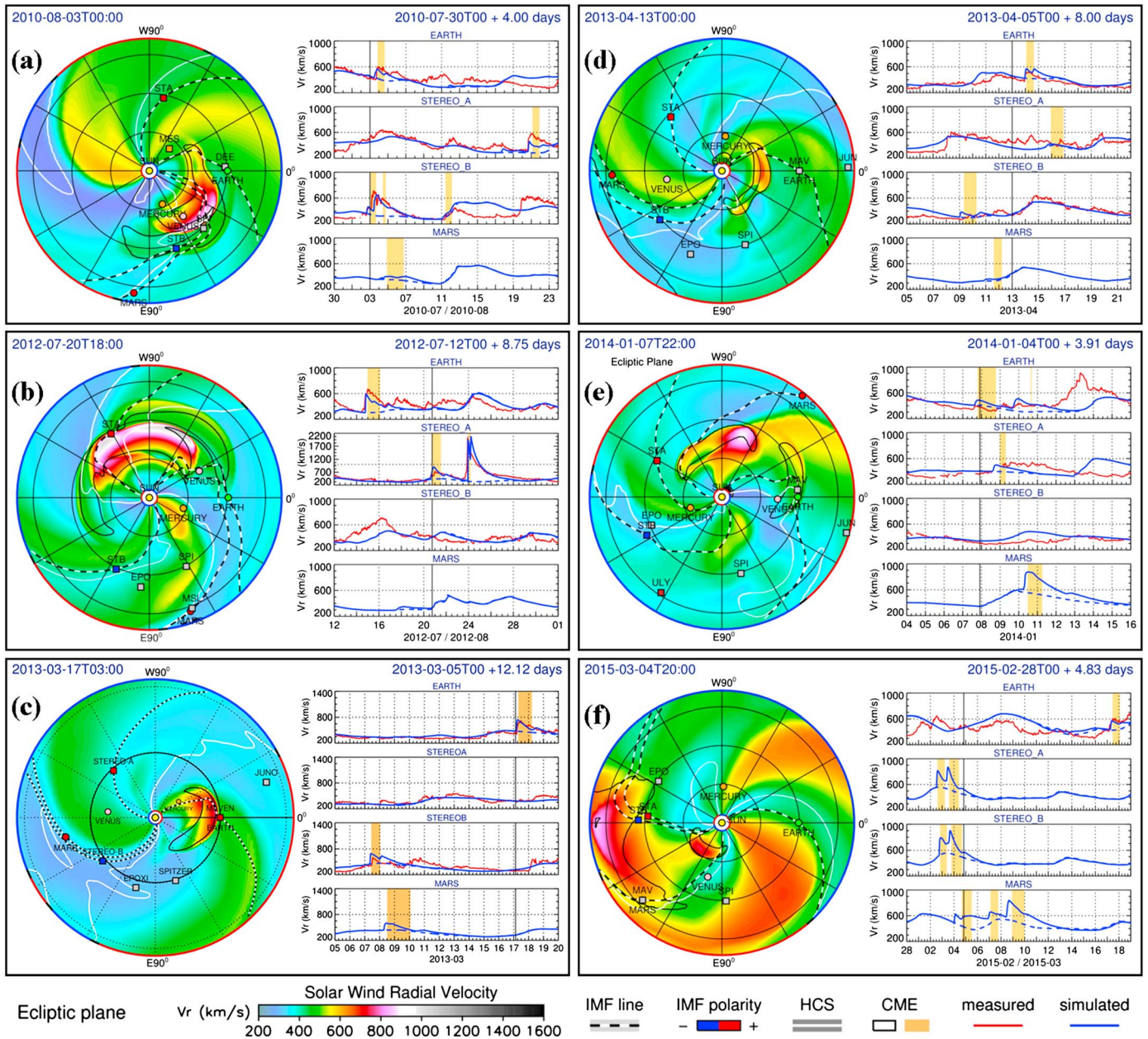


Figure 1. Snapshots from the ENLIL runs used in the present study. Each of the six cases are illustrated by an ecliptic contour map on the left showing the simulated solar wind radial velocity, including both the ambient stream structure and one or more of the cone model ICME transients in the run (usually the red areas indicating the highest velocities). The date and time represented by the contours is on the upper left. Interplanetary magnetic field polarity at the circular boundary is specified by red (+, outward) or blue (−, inward) color. The speeds the contour colors represent are indicated by the scale at the bottom, while observer connected field lines at the time of the snapshot, for Earth, STEREO A/B, and Mars, are shown as dashed lines. On the right, the simulated radial velocity (V_r) time series for the full ENLIL run are plotted for each of these observers as solid blue lines, with the dashed blue lines showing model results without the cone model ICMEs. The corresponding plasma velocity observations at ACE and the STEREO sites, when available, are shown in red. The vertical black line marks the time of the color contour snapshot. Gold-colored bars superposed on the time series, usually following ENLIL shock arrivals, mark the passage of the material in the cone model CME gusts. In considering these examples, note that the physics of SEP events is such that SEPs at an observer’s location may come from remote connections to ICME shocks that are not detected in situ. Thus, SEP time series are not necessarily directly interpretable from these V_r time series by themselves. (a) The ENLIL results for a period of multiple CME activity in August 2010, discussed in more detail in *Bain et al.* [2016]. (b) Results for an especially active period in July 2012, during which STEREO-A observed one of the more extreme ICME events on record. *Bain et al.* [2016] also discuss this period. Note that the separation of the spacecraft in this case was such that the major ICME (largest velocity jump in the time series) was mainly at STEREO-A’s location—although as will be seen later, the SEPs exhibit a greater longitudinal spread. (c) Same as Figures 1a and 1b but for March 2013 when a relatively isolated Earth-directed eruption occurred. (d) Same as Figures 1a–1c but for a period in April 2013 when different relatively weak ICMEs (gold bars in the V_r time series) passed the different observers. (e) Same as Figures 1a–1d but for a period in January 2014. As discussed later in this paper, this period produced a noteworthy SEP event at Earth but only a modest ICME signature. (f) Same as Figures 1a–1e but for a period in March 2015 when superior conjunction operations on STEREO interrupted the regular data acquisition at those sites.

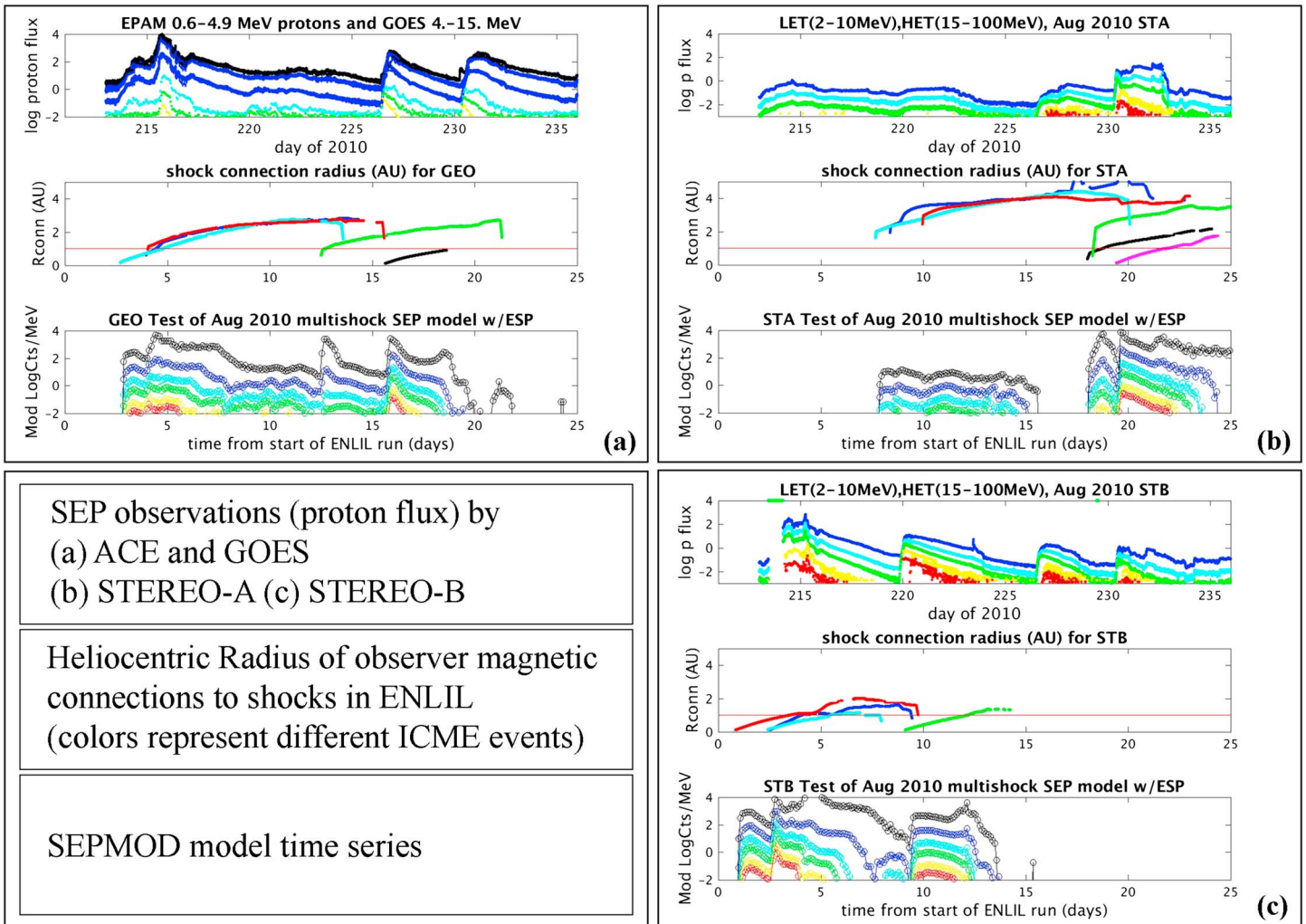


Figure 2. (a) Time series of the SEP activity observed from 1 to 21 August 2010 as seen in ACE (EPAM) and GOES 1–100 MeV energetic protons (top panel, fluxes in units of protons/(cm² s sr MeV)); ENLIL results for the simulated ICME shocks during this period, showing the heliocentric radius of the (Earth-GEO) observer (red line) and the radius R_{conn} of the field line connection to each shock (distinguished by color; middle panel); and the results of the SEPMOD calculations for the same proton energy range as the data and on the same (log) differential flux scale, based on the ENLIL results. Note the timescale for the data in the top panel is in day-of-year, while the timescale for the two model panels below is the time from the start of the ENLIL run. In both the data and model time series, black represents the lowest energies ~1 MeV and red the highest energies. The model flux time series are in all cases shown for 1.2, 2.6, 5.1, 8.6, 17, and 26 MeV. (b) and (c) Same as Figures 2a but for STEREO-A (STA) and STEREO-B (STB) whose locations relative to Earth at this time can be seen in Figure 1a.

or more cone model CMEs once the setup phase is over, together with the relative positions of three 1 AU observation points at Earth, STEREO-A, and STEREO-B at the time. One can see from these examples that these observers were increasingly separated in the time span between the earliest event period analyzed in August 2010 and the latest in March 2015. The quality of agreement of the ENLIL results with the in situ time series of the solar wind velocities at STA, STB, and ACE (Earth) provides a visual measure of the success of the ENLIL run in predicting both the plasma speed and ICME arrivals. The passages of the ENLIL ICME “drivers” at the observer locations, representing the local counterparts of the high-pressure initially spherical plasma gusts erupted at the inner boundary, are indicated by the gold-shaded intervals. As seen here, ENLIL is able to capture at least major ICME features including arrival times in most of the cases shown. These represent the minimum presumed locations where structures such as magnetic cloud flux ropes—not in these simulations at present—would be observed. As a result, details of the modeled SEP time profiles around these intervals are not expected to exhibit the effects of any such ejecta inclusions.

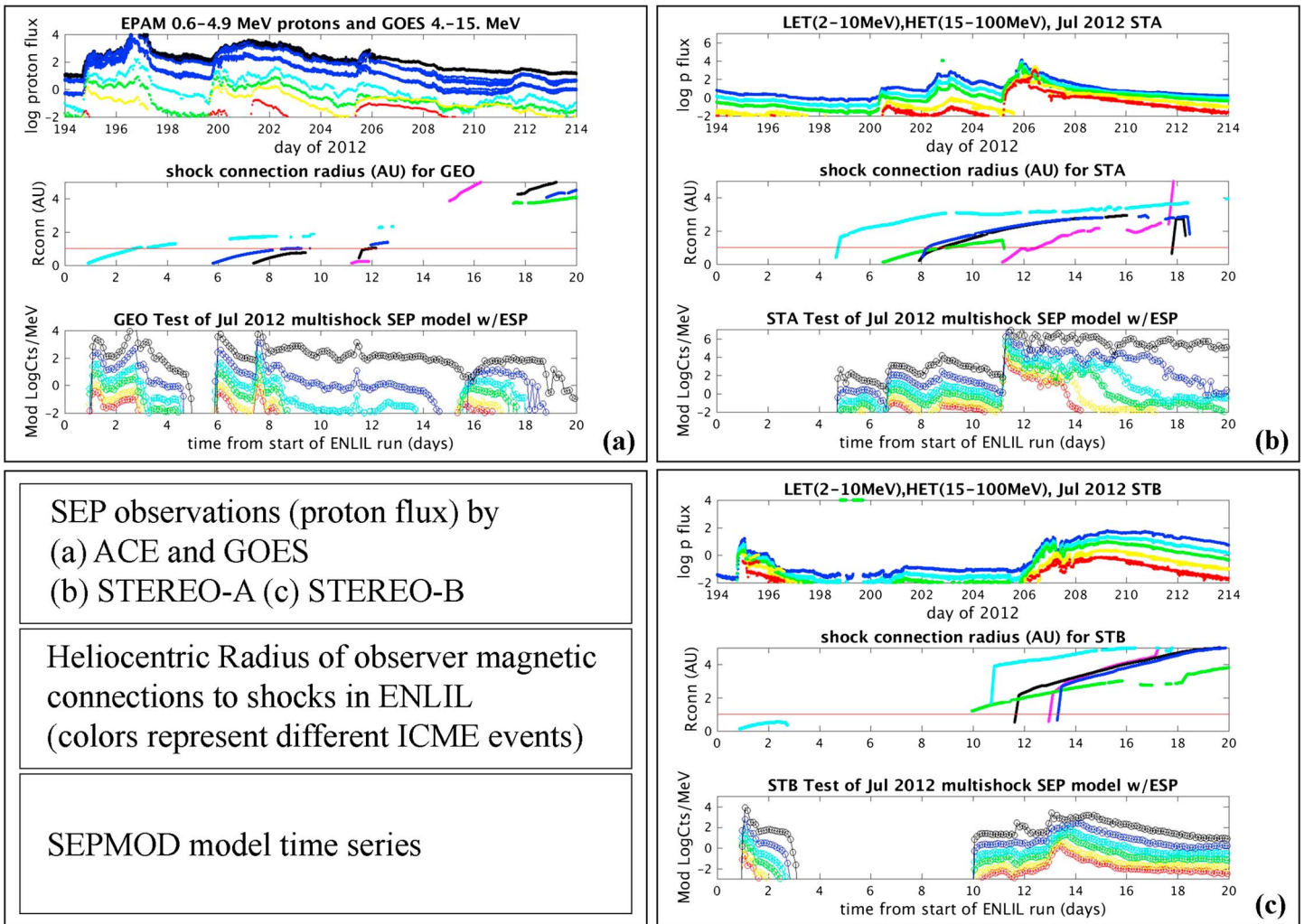


Figure 3. Same as Figure 2, but for the period 12–31 July 2012. The relative locations of the three observing points at this time for (a) Earth (GEO), (b) STA, and (c) STB can be seen in Figure 1b.

Also seen in these figures are the ENLIL magnetic field lines through the observers at the time(s) of the snapshots (Mars results are shown as an additional point of information, relevant to future uses). These pictures change as the shocks move through the simulation grid to its outer boundary at 5.5 AU. In general, the periods chosen include multiple cone model CME injections. The resulting disturbances often merge with the background solar wind structure, as well as with each other as they propagate outward. Observer field lines can also intersect more than one disturbance at a particular time, producing conditions for multiple source contributions plus additional magnetic mirroring effects in the SEPMOD SEP events. However, one must bear in mind that the lack of ejecta magnetic fields in these pictures, noted earlier, affects the resulting SEP profiles in ways not controlled by SEPMOD itself. One particularly important point these field lines illustrate is the significant departures from Parker spiral geometries that can be present during SEP events. Another important point is that it is difficult to validate the ENLIL results anywhere but at an observer's location. In a way, the SEP data comparisons and calculations present a kind of long-baseline, remote location validation.

3.2. Observed and Modeled SEP Time Profiles at 1 AU

Figures 2–7 show 1 AU SEPMOD results for the selected event periods (bottom panels), together with 5 min resolution SEP proton observations from STEREO-A and STEREO-B (STA, STB) LET and HET instruments [Mewaldt *et al.*, 2008; von Rosenvinge *et al.*, 2008], EPAM on ACE [Gold *et al.*, 1998], and GOES EPS fluxes (1 h resolution) from the OMNI database (<https://omniweb.gsfc.nasa.gov>) (top panels). The typical time

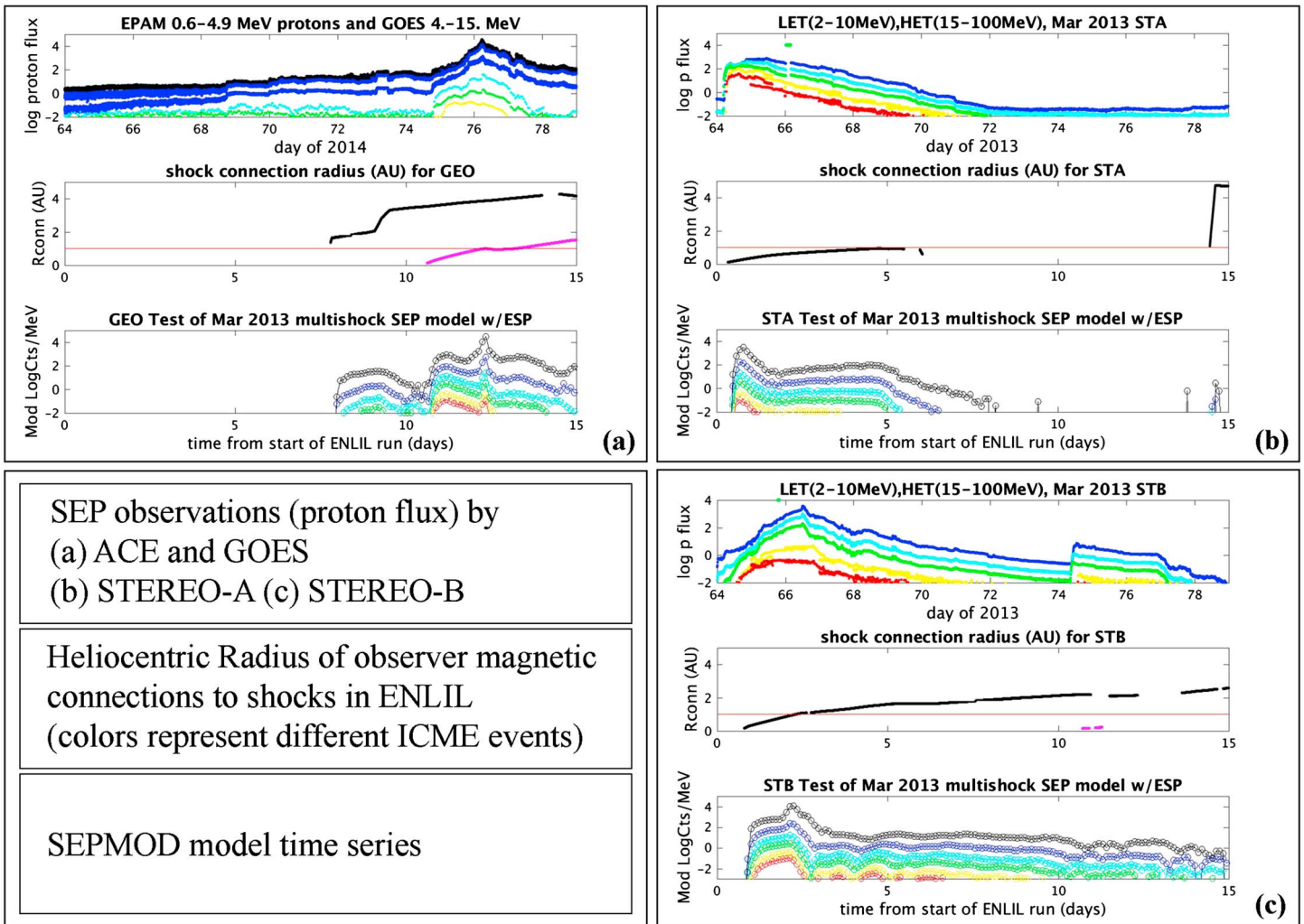


Figure 4. Same as Figure 2, but for the period 5–20 March 2013. The ENLIL results in Figure 1c show the geometry of the three observers at (a) Earth (GEO), (b) STA, and (c) STB.

spans covered by the ENLIL runs for these cases are ~20 days. Separate plots represent the three observer locations. The observed SEP time series are plotted for a range of proton energies from ~1 MeV to ~100 MeV to provide a broad view of the SEP fluxes present over the time covered by each ENLIL run. The corresponding SEPMOD plots in the bottom panels show SEPMOD SEP flux time series results on the same flux scale as the observations. However, for the display of the model results, we use a fixed uniform sampling in proton energy over the range that covers the observations shown but is not instrument or mission-specific. Similar colors are used for similar energies in the observed and model SEP time series.

The middle panels show ENLIL shock file results that are especially useful for interpreting the SEPs in the time series. These give the heliocentric radius (R_{conn}) of the observer magnetic connections to the shock for each CME (identified separately by color). This also indicates the relative timings of the shock connections, which may not coincide with the time(s) of the CME(s) and/or ICME(s) (see Figures 1a–1f). The horizontal red lines mark the 1 AU observer heliocentric radius. Shock connections located below this observer line occur between the Sun (or ENLIL inner boundary at $21.5 R_S$) and the Earth, while connections above it occur beyond the observer heliocentric distance out to the 5.5 AU boundary of the ENLIL simulation. Notice that the time spent connected to the shock beyond the observer often exceeds the time spent connected inside 1 AU, with the implication that the calculated event time span can be affected by outside connections. Traces that cross the 1 AU line imply that there is in situ observation of that shock (as seen in Figures 1a–1f) and a possible ESP

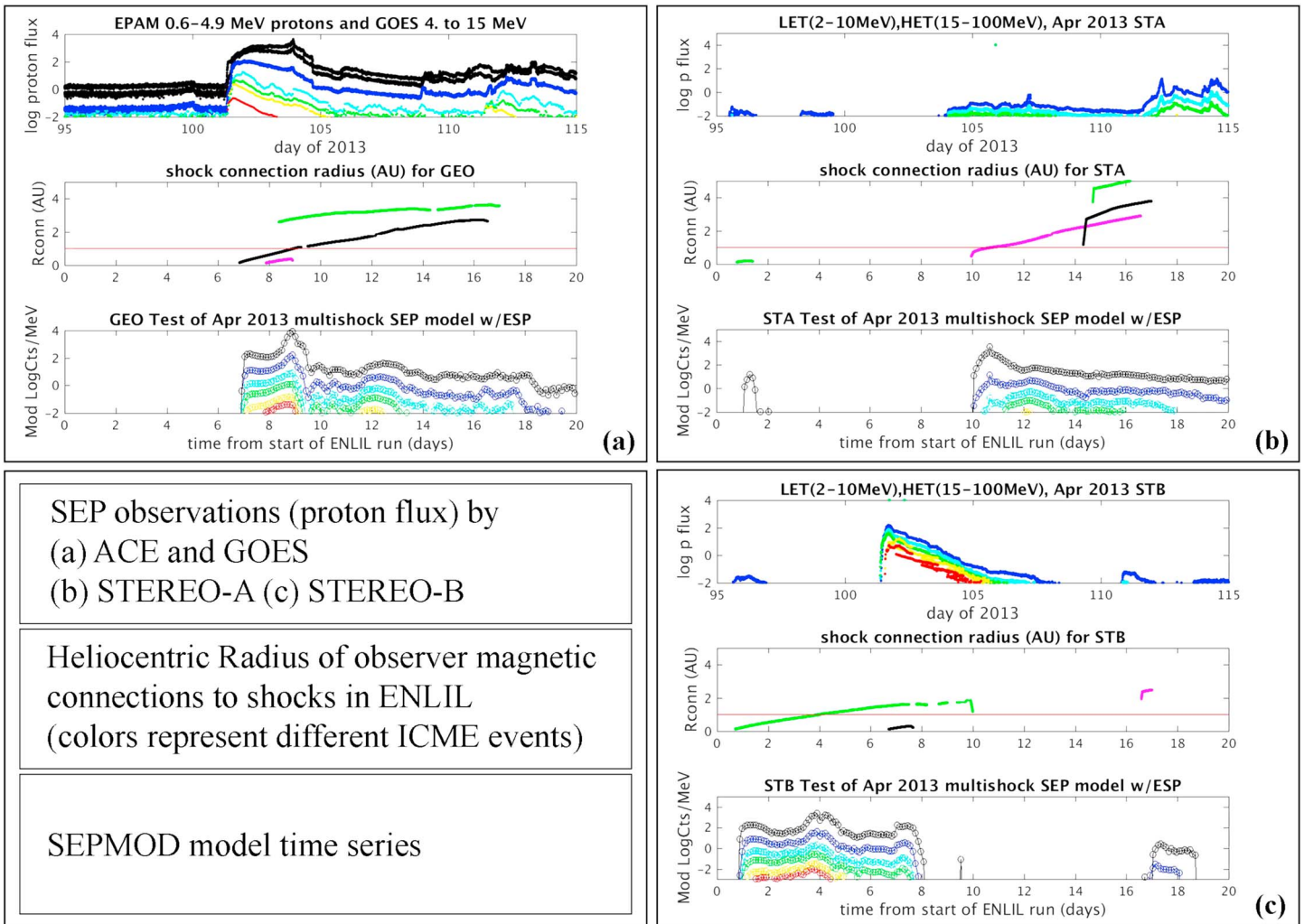


Figure 5. Same as Figure 2 but for the period 5–25 April 2013. The ENLIL run results for this period, showing the locations of the three observing sites represented here: (a) Earth-GEO, (b) STA, and (c) STB, can be seen in Figure 1d.

enhancement as part of that particular SEP event contribution. Also of interest are the events that are completely determined by remote shock connections according to the ENLIL results, as well as events whose identity can be complicated by the presence of multiple shock connections at the same time. For the selected study periods, there are often more ICME shock connections than ICMEs seen in situ at the observer (see the gold bars in Figures 1a–1f). Many of these are only remote, distinguished by shock connection radius traces that do not cross the red 1 AU line. Note that some of these connections start near the inner ENLIL boundary (near $R_{\text{conn}} = 0$ on this plot), while others start at a variety of heliocentric distances out to the 5.5 AU limit of the heliospheric model. Thus, many new shock source connections are spatial, implying that the observer connects to fields already occupied by SEPs—rather than originating at a newly formed shock on the observer field line.

Several caveats are in order in comparing the observed and modeled results. For example, explicit descriptions of the coronal disturbance and ejecta fields are not included in ENLIL cone model CMEs, limiting the amount of detail that can be reproduced. This especially affects cases where near-Sun shock connections occur and also in the post-shock period of the resulting ICMEs. In particular, the introduction of the cone model-related ICME disturbance at the 21 R_s ENLIL inner boundary is abrupt, making the associated early shock both likely to be influenced by startup issues and difficult to characterize. As a result, some near-Sun shock connections may produce overly abrupt, strong-modeled SEP flux onsets. Later observed SEP time

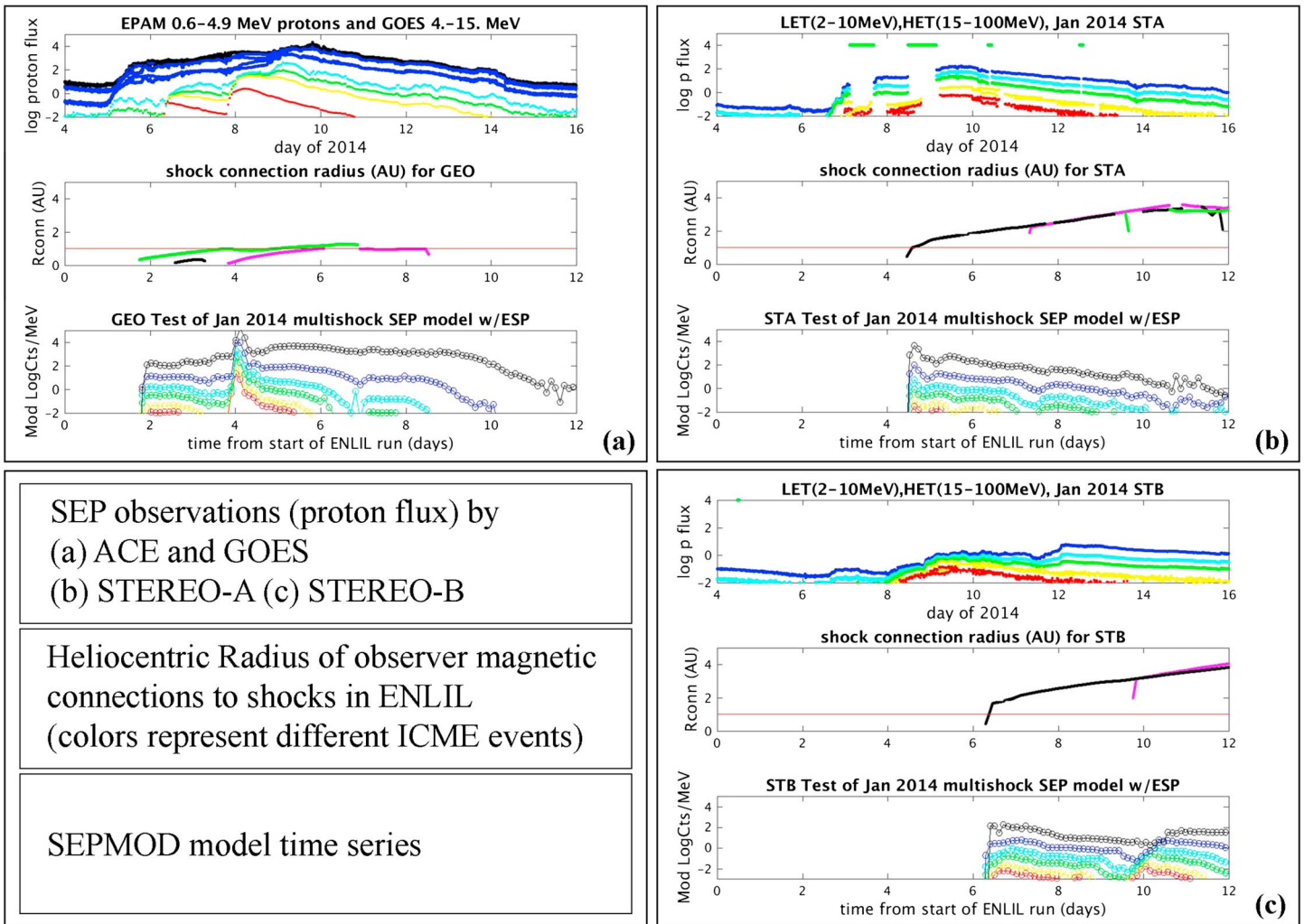


Figure 6. Same as Figure 2 but for 4–16 January 2014. The ENLIL results for this period, showing the locations of the three observers at (a) Earth-GEO, (b) STA, and (c) STB, can be found in Figure 1e.

profiles coinciding with ICME arrivals sometimes show a period of decreased fluxes during ejecta passage, suggesting those fields form a barrier to the surrounding energetic protons. The ejecta field omission is also expected to affect both the shape of the shock and its evolution but is an understood attribute of the WSA-ENLIL-cone heliospheric model external to SEPMOD. Along these lines, it is worth noting here that while the absence of the coronal shock portion will compromise the SEPMOD SEP event onset timing in cases when the observer is connected to a shock that forms right at the boundary, it will not affect the onsets that occur due to new observer connections to existing shocks that are already established within the ENLIL domain (e.g., “geometrical” onsets), or when the shock forms in ENLIL at a distance from the inner boundary (as what happens in the cases of initially moderate speed CMEs). Additionally, the scatter-free propagation and guiding center motion that are part of the SEPMOD version used here are to be regarded as part of the assumptions under evaluation. If scattering, especially as it relates to perpendicular (to the field) diffusion, is an important determiner of the gradual SEP time profiles, the shock source connection histories will be insufficient for modeling the event appearances. On the other hand, if the event time profiles are well represented, the results can be interpreted to mean that the observer field line connection to the shock source and its evolution dominate their main characteristics. Of course, this does not preclude the essential role of scattering within the shock source itself—implicit in a number of SEPMOD assumptions—including the SEP injection spectrum based on the *Jones and Ellison* [1991]

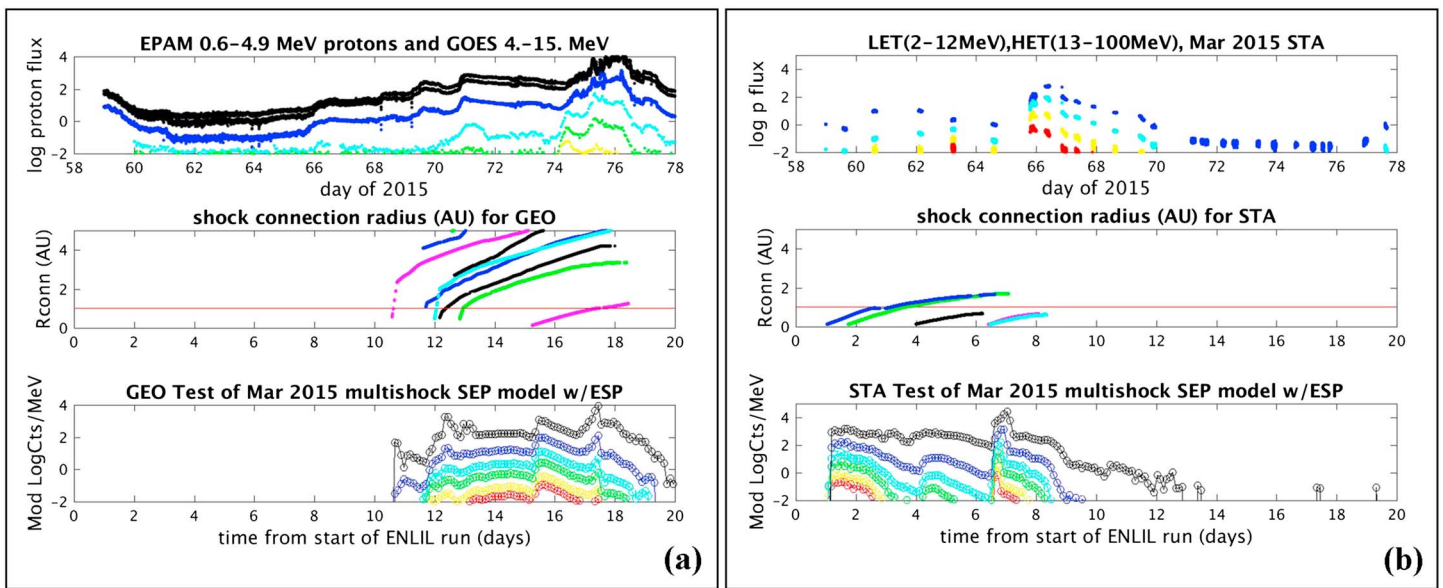


Figure 7. Same as Figure 2 but for 28 February to 19 March 2015. At this time, STEREO was undergoing special superior conjunction operations that limited the available data (with no data available from STB). The relative locations of the observers at (a) Earth-GEO and (b) STA, represented by the time series above, are illustrated in Figure 1f.

diffusive shock acceleration formula and the inclusion of the additional ESP component in the vicinity of the shock [see *Luhmann et al., 2010*].

The main aim of SEPMOD is to simulate the observed occurrence and timing of SEP events, as well as their fluxes, durations, and spectral variations within the time periods of the heliospheric models. In discussing these plots for each time period, we focus on a few key types of behavior found in the data and their model counterparts. These include the following: (1) Events having rapid onsets—sometimes with contributions from higher energy protons—whose intensities then exponentially decay within a day or two thereafter are generally associated with model field connections to shocks starting close to the Sun. This is consistent with the picture of *Cane et al. [1988]* where the observer field connection to a shock source near the west limb of the solar disk is lost early because it propagates outward too far west of the observer’s location for the connection to be maintained out to 1 AU. (2) Events that cross the red 1 AU line. These are usually associated with the gold bars in Figures 1a–1f, indicating that the ICME’s path crosses the observer. These more centrally located (from the observer’s viewpoint) ICMEs—including those related to local halo CMEs—often produce the longest duration events because they allow sustained observer connection to the shock source. Finally, (3) SEPs from connections to the backside of a shock after the ENLIL disturbance have moved beyond the 1 AU observing location, often neglected in SEP time series interpretations. These three types, and combinations of them, help to untangle the complex, multiple event time series described here.

3.2.1. The August 2010 Events

Bain et al. [2016; also see Rouillard et al., 2011] describe the various solar events contributing to the period spanning 1 to 21 August 2010. The Earth (GEO) and STB observing points (Figures 2a and 2c here) experienced the most SEP activity, as seen in the top panels. According to the ENLIL results, the earliest and strongest events near the beginning of these time series started with shock connections that occurred close to the Sun (see the blue, black, and cyan traces in the middle panels showing the heliocentric radial distances of the individual ENLIL shock connection points). For these events, the local encounter with the shock, also indicated by these traces crossing the horizontal red “1 AU” line, further increased the local SEP fluxes with ESP enhancements at both Earth and STB. In addition, at STB the relatively long duration of the shock connection radius at 1 AU extended the period of this enhancement. The situation at STA is suggested by the model to have no shock connections to the earliest ICMEs, to have been connected to shocks well beyond 1 AU for several events in the center of the time period, and to have had the most productive, inner heliosphere shock connections, for the later events. The SEPMOD results in the bottom panels, based on the ENLIL shocks

and observer field line connections, are plotted in the bottom panels for proton energies 1 to 75 MeV, spanning those covered in the ACE and STEREO measurements in the top panels. While the colors of the SEP time series in the measurements and the model results do not represent exactly the same energies, their similarity allows visual comparisons of the two, as well as interobserver comparisons. Overall, the SEP time variations and flux/energy trends between the two are consistent, with the notable exception of the two smaller events in the second half of the observed time series at STB. These “missed” SEP events are interesting in that they illustrate one possible consequence of the ENLIL 21.5 R_s inner boundary. These two events produced modeled counterparts at Earth and STA (see Figures 2a and 2b, middle panels), although they are too early at Earth. However, they are not captured in the model shock connections for the STB observer (or in the second case, also for the Earth observer) because the inferred magnetic field connections for this location are inside 21.5 R_s . Thus, an ENLIL and SEP MOD user without any other information would be able to approximately describe the SEP time histories observed at 1 AU for this period, with these two exceptions (see *Bain et al.* [2016] for additional discussions of this period’s events and shock connectivities).

3.2.2. The July 2012 Events

The in situ observations and ENLIL simulation (see Figure 1b) for the 12 to 31 July 2012 period were also described in detail in *Bain et al.* [2016]. It is widely recognized [e.g., *Russell et al.*, 2013; *Liu et al.*, 2014] that the period shown in Figures 3a–3c includes one of the most extreme episodes of space weather for which we have a fairly complete record of multipoint plasma, magnetic field, and SEP data, plus multiperspective images. The strongest solar event, a CME on 23 July (day of year 205), was most centrally observed and sampled on STA. It is possible that the severity of this event was enhanced by several preceding weaker CMEs from the same general region in the corona, whose ICMEs helped clear the path for the subsequent faster, larger ICME [e.g., *Liu et al.*, 2014]. The SEPs from these preceding ICMEs can be seen from the two smaller onsets in the days before the strongest SEP event in the STA time series (Figure 3b). As indicated by the middle panel, the ENLIL simulation for this period captured the prior shocks from these earlier events. From the SEP MOD results in the bottom panel, it can be seen that the STA connection to the strongest shock in the simulation (magenta trace) occurred at the ENLIL inner boundary, close to the Sun, and that the observed SEPs peaked when the shock arrived at the observer. The speed of the shock for this ICME was exceptional and sustained [e.g., *Liu et al.*, 2014], with observed speeds of over several thousand kilometers per second in the corona and ~ 1700 km/s at 1 AU. The magnitude of the shock jump (see Figure 1b, STA V_r time series) made this event an exceptionally strong SEP source by itself, but its SEPs were generated on top of SEP events from the previous, weaker ICMEs mentioned above. Thus, in many ways the conditions at STA were the “perfect storm” setup for near-record SEP fluxes to occur. While the detailed shapes of the flux variations in the SEP MOD time series only approximately capture the details of the observed extreme SEP event seen on STA, the maximum flux levels and the timings of SEP increases are compatible at the higher energies shown. The observations and model results for STB in Figure 3c show that these same ICMEs also affected conditions at STB, although much of STB’s shock connectivity occurs outside, rather than inside, of 1 AU where the shock source continued to weaken. The situation for Earth (GEO observer in Figure 3a) was considerably different due to its large longitudinal separation from STA and its major activity corridor. Here the proton fluxes at the lowest energies are overestimated in SEP MOD results for several of the near-Sun (small R_{conn}) shock connections. While it appears that the weaker, earlier ICME shocks were magnetically connected to the Earth observer, the connection to the strongest shock in ENLIL for the period was brief and weak. As a result, the sustained SEP fluxes at Earth over this period came from mainly interior (to 1 AU) connections to a few more modest ICME shock sources spread out through the first half of the overall period. In keeping with these results, SEP MOD time series (bottom panels) show almost no effect of the major halo CME-generated shock affecting STB and Earth (GEO). SEP MOD results are also consistent with the low SEP activity leading up to the STA major events (Figure 3b) and with the gap in SEP activity seen on STB following a brief event at the beginning of the study interval (Figure 3c). Note that instrument background subtractions have not been made in the observed fluxes shown here and elsewhere nor is any correction made for residual SEPs generated by solar events earlier than the ENLIL run time windows.

3.2.3. The March 2013 Events

In contrast to the above periods, 5 to 20 March 2013 represents a relatively simple time with only two CMEs included in the ENLIL run (Figure 1c). Moreover, the ENLIL magnetic connectivity results (Figures 4a–4c, middle panels) indicate that only the Earth observer (Figure 4a) was affected by both ICME shocks, while STA and STB (Figures 4b and 4c) had long-duration connections to the same single ICME. This period provides an

opportunity to contrast the previous cases against one with fewer, more isolated events. At STA (Figure 4b), an early close-to-Sun connection is established to a fairly strong shock, causing a sudden SEP onset in both observations and SEPMOD results. The shock connection trace in the middle panel below the observed time series indicates the shock connection asymptotes to 1 AU and then ceases. SEPMOD results show a flattening of the modeled flux decay profile here, related to ongoing ESP flux enhancements in the vicinity of the shock. In contrast, the observations show a relatively smooth decay with only a hint of slope change toward the end. This example may represent a case where the neglect of the field structure in the real shock driver (the ICME ejecta) is affecting the results in an especially visible setting, or equivalently, where SEPMOD's simplified description of the ESP flux enhancement around the shock crossing is not adequate. And while the modeled event flux, spectral evolution, and duration are not unreasonable, SEPMOD's modeled energy spectrum is too soft. Nevertheless, the STB case (Figure 4c) flux levels and time history are approximately reproduced, including the longer-duration SEP event due to the longer-duration ICME shock connection. At Earth (Figure 4a), where the observer connects to both ICME shocks, it appears that the onset of the second ICME contribution, indicated by the magenta trace in the middle panel, is stronger than what is observed, although the timing of the modeled ESP enhancement coincides with the observed event peak. In considering this and other relatively simple cases, it is important to remember that attempts to capture details of solar wind structure as well as the injected CMEs in ENLIL alone are fraught with challenges [e.g., Mays *et al.*, 2015a, 2015b, and Figure 1]. The modeled SEP events are inextricably tied to these.

3.2.4. The April 2013 Events

The 5–25 April 2013 period studied is similar to the preceding March 2013 period in its inclusion of just a few CMEs. The related SEP activity has been featured in multipoint studies using well-separated spacecraft [e.g., Cohen *et al.*, 2014; Lario *et al.*, 2014]. The SEPMOD results analogous to those shown above bring out one particularly glaring “miss” in the case of the STB observer (Figure 5c). How much of this miss is due to the ENLIL shock and field simulations versus SEPMOD assumptions is revealed in part by the middle panel in this case. ENLIL found an early and close-in shock connection (green trace) that lasted most of the first day and continued after shock passage for several more days. SEPMOD predicted moderate SEP fluxes at STB from this shock source (Figure 5c, bottom panel). However, SEPs at the modeled level are not observed at STB up to the time of the near-Sun shock connection shown by the black line in the middle panel. This second, close-in, brief modeled shock connection (black trace) is associated with a significant, sharp sudden onset event seen on STB. This is the classic profile for an early, strong, western limb event connection to a shock close to the Sun, but in the SEPMOD results, the brief ENLIL shock connection at small R_{conn} (Figure 5c, middle panel, black trace) produces only a modest increase during the already ongoing modeled SEP event decay phase. SEPMOD produces no SEPs for the duration of the subsequent observed STB event and then a weak onset for a final connection to a last shock source beyond 1 AU. In this case some combination of the ENLIL shock descriptions and the inner boundary location (e.g., ability to simulate near-Sun ICME shocks) largely determined the missed predictions by SEPMOD. This finding is particularly important considering the next study period, which included one of the very few GLEs of cycle 24.

3.2.5. The January 2014 Events

The period between 4 and 16 January 2014, like the preceding two intervals, had a limited number of events that produced rather weak (observed and modeled) shocks at the 1 AU observer sites as seen in Figure 1e. However, it included one of the few GLE events of the cycle 24 maximum, on January 6 [see Thakur *et al.*, 2014; Gopalswamy *et al.*, 2015]. This event corresponds to the second energetic proton peak in the GOES data in the top panel of Figure 6a and to the ENLIL model magenta R_{conn} trace (middle panel) indicating a near-Sun magnetic connection of Earth's location to a shock. The implication is that the responsible strong ICME went off toward the western sector of the heliosphere as seen from the Earth, barely grazing or missing the Earth but heading toward Mars. This idea is confirmed by the ENLIL model of the solar wind at Mars, which produced the simulated velocity time series in the bottom panel of Figure 1e where a strong ICME signature is seen [see discussion in Mays *et al.*, 2015b]. This event period was previously analyzed in detail by Moestl *et al.* [2015], who used a different approach to analyzing the CME expansion and propagation but came to the essentially same conclusion. In addition, these authors analyzed Mars Express plasma electron analyzer measurements and found the signature of an arriving ICME on 11 January. They also identified the counterpart of a Forbush Decrease in the local galactic cosmic rays starting at that time and lasting several days in the Mars Science Laboratory (MSL) RAD detector data. This ICME arriving at Mars is likely the one associated with the GLE event which lacked an apparent later ICME arrival at Earth (black R_{conn} trace in Figure 6a). Overall, this

information confirms the geometric interpretation invoked for most GLEs, which are extreme examples of western disk events for which a SEP event is detected but the ICME misses the observer. We return to this case for more discussion later. However, it is worth mentioning the relationship of this case to those of the August 2010 STB observations and model (Figure 2c) and the April 2013 STB observations and model (Figure 5c). These were both cases where close-in shock connections seem to have compromised the use of SEPMOD. However, in this January 2014 case, SEPMOD does produce a flux enhancement at the time of the GLE, suggesting that whether or not it (at least partially) captures events that are primarily near-Sun shock connections is case-specific.

3.2.6. The March 2015 Events

A period of activity in late February into late March 2015 (28 February to 19 March) sparked special interest because a number of events occurred on the farside with respect to the Earth as the STEREO spacecraft were in the beginning phases of a period of non-operation during superior conjunction. STB had earlier (October 2014) experienced an anomaly and was no longer communicating, while STA was working on a reduced data transmission level—although still obtaining beacon-grade images and in situ observations. A large number of CMEs were observed and produced remote shock connections to Earth's location in ENLIL results, although mainly to shocks beyond 1 AU—as seen in the middle panel of Figure 7a. In contrast, as seen in Figure 7b, only four ENLIL shocks connected to STA from inside of 1 AU in the first few days of March (see Dewey *et al.* [2016] for an earlier description of this ENLIL run period). The SEPs produced by these shocks, shown in the top panel, appeared as a sequence of two significant flux increases, also seen in the SEPMOD simulated time series in the bottom panel. One other reason for interest in this period is that Mars was also at large longitudinal separation from Earth, and MAVEN's SEP detector was available to provide a third observer, in this case at the larger heliocentric distance (~1.5 AU) of Mars. We consider the MAVEN observations in the context of describing samples of other applications of SEPMOD (besides the Earth and STEREO observation interpretations) below.

3.3. Examples of SEP MOD Applications

3.3.1. MAVEN SEP Event Observations at Mars

MAVEN has been in orbit around Mars since late 2014 [Jakosky *et al.*, 2015]. Its instrumentation includes a full complement of space plasma and particle detectors, one of which detects SEP ions (~20 keV to ~6 MeV) and electrons (~20 keV to ~200 keV) [see Larson *et al.*, 2015]. One of the strongest space environment storms observed on MAVEN was on 6 March 2015, when it detected a moderately fast ICME both preceded by and accompanied by SEPs [see Lee *et al.*, 2017]. According to the ENLIL model for the period surrounding this event [also described in Dewey *et al.*, 2016], illustrated in Figure 8a for a time when one ICME is inferred to have brushed by Mars, the Earth observer was magnetically connected to many shocks in the latter half of the simulation period (see Figure 7a, middle panel). However, most of these were weak shocks already having passed 1 AU. The analogous results for the Mars observer, shown in Figure 8b, suggests that at least a few of those shock connections at Earth were to the same shocks experienced earlier at Mars. The Mars interplanetary field connections were primarily to shocks inside the orbit of Mars at the time, some near the ENLIL inner boundary. The ~1 MeV to ~6 MeV SEP ion fluxes observed at Mars (Figure 8b, top panel) can be compared with the SEP MOD fluxes (Figure 8b, bottom panel). SEP MOD takes into account the radial divergence of heliospheric flux tubes in calculating the fluxes from the ENLIL shock sources. However, while the SEP MOD flux levels are moderately consistent with those observed on MAVEN, one of the main issues with this comparison stems from the large number of shock sources that Mars is connected to in the ENLIL results. The MAVEN SEP time profile more closely resembles that observed on STA (see Figure 7b), which had notably fewer shock connections over the same time period, although STA and Mars were separated by only ~45°. Figure 8a illustrates one possible explanation for the difference. A number of the ICME shocks in this ENLIL run appear to merge with each other and with stream interaction region compressions by the orbit of Mars. Indeed, many of the Mars shock connections in Figure 8b (middle panel) seem to hover around the red line marking Mars' radial distance. The relative location of STA to the East of Mars tends to not necessarily favor the same connections for the same reason that Eastern disk eruptions seen at the Sun as viewed from Earth often produce no or weak SEP events at Earth. This result suggests how ENLIL with SEP MOD may be useful for both Mars SEP event interpretations (including MSL RAD measurements on the ground [Hassler *et al.*, 2014]) and for demonstrating a potential tool for human mission applications [also see Aran *et al.*, 2007].

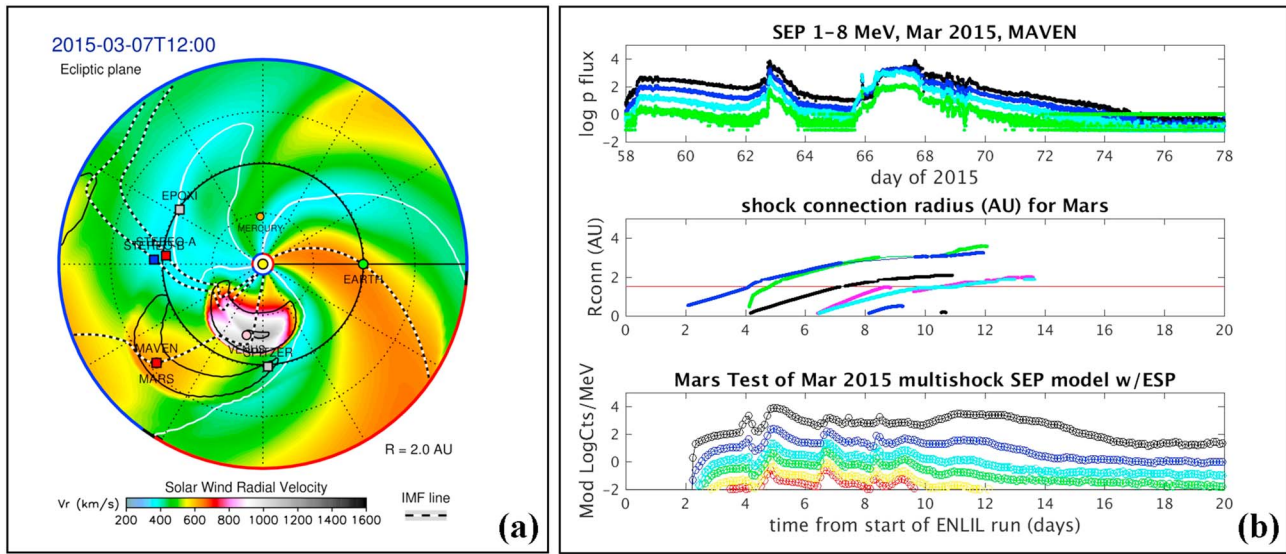


Figure 8. (a) An ENLIL model snapshot of the scaled solar wind density in the ecliptic plane (left, from <http://ccmc.gsfc.nasa.gov/iswa/>) suggests the heliospheric conditions at the time a major SEP event and ICME was observed at Mars (red circle at ~1.5 AU from the Sun) on MAVEN. (b) The MAVEN SEP detector results for 28 February through 19 March are shown in a display similar to those in Figures 2–7. The ENLIL shock connections in the middle panel are for Mars in this case, with the red line marking 1.5 AU. SEPMOD results for a Mars observer are shown in the bottom panel.

3.3.2. Venus Auroral Activity Interpretations

One method of remote planetary space weather is by detection of auroral activity. For example, HST (Hubble Space Telescope) has been used to detect UV auroral ovals on both Jupiter and Saturn [e.g., see *Clarke et al.*, 2005, and references therein]. These aurorae were inferred to respond to solar wind disturbances, evidently brightening when a high dynamic pressure enhancement impacts the planet’s magnetosphere. More recently, *Gray et al.* [2014] reported ground-based telescope observations of visible auroral green line emissions at unmagnetized Venus. A diffuse nightside UV aurora, whose brightness intensified with solar wind pressure enhancements, had previously been detected from the Pioneer Venus Orbiter [e.g., *Phillips et al.*, 1986]. *Gray et al.* [2014] related the occurrence of their detected green line emissions to the eruptions of coronal mass ejections observed by heliospheric observatories, traveling toward Venus. When MAVEN arrived at weakly magnetized Mars in late 2014, it carried a UV spectrometer that detected diffuse nightside emissions found to coincide with the arrival at Mars of energetic solar electrons [*Schneider et al.*, 2015]. The connection of SEPs with coronal mass ejections raises the question of whether the Venus aurorae are similarly SEP associated. Although there have been no direct SEP measurements on Venus missions, the Venus Express orbiter carried a plasma spectrometer (ASPERA-4) [see *Barabash et al.*, 2007] that has backgrounds sensitive to the local radiation environment [*Futaana et al.*, 2008]. We can investigate this question of a Mars-like SEP connection of the Venus aurora using these data and SEPMOD verification of the presence of SEPs at Venus at the times the green line aurora are observed.

Figures 9a–9c includes three standard time series displays for periods of interest in this paper, during which the Venus Express ASPERA-4 Ion Mass Analyzer backgrounds (plotted in the top panels in lieu of SEP data) showed enhancements in the local radiation environment. *Gray et al.* [2014] conducted telescopic observations during one of these periods (in late July 2012) and found enhanced green line emissions. The ENLIL shock connections at Venus in the middle panel suggest when SEPs might be present, with time series possibly like those calculated with SEPMOD—in the bottom panels. While the particle energies responsible for the ASPERA-4 backgrounds are not clear, the qualitative resemblance of their intensity time histories with the modeled energetic SEP proton fluxes is consistent with a relationship. While the Mars UV diffuse auroral observations are more closely connected with SEP electron than SEP proton fluxes there, SEP electron time series trends generally follow those of the energetic protons. The implication is that ENLIL and SEPMOD provide a means to remotely monitor SEP presence and related effects at the planets, even without a local source of information.

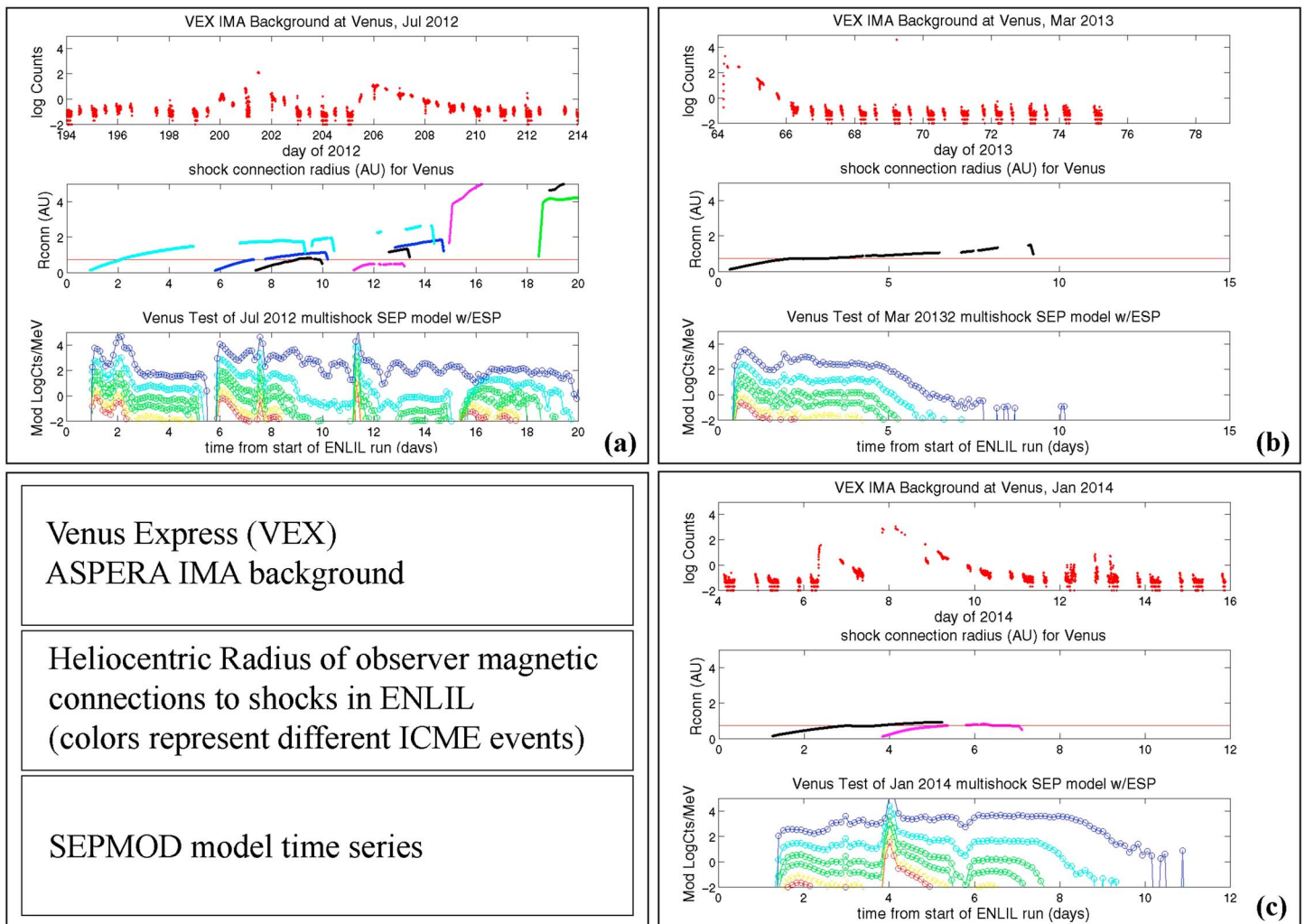


Figure 9. Examples of plots analogous to those in Figure 2 from a subset of cases where Venus Express ASPERA detector backgrounds (top panel) serve as substitutes for direct SEP observations. These are for three periods analyzed in this paper: (a) July 2012, (b) March 2013, and (c) January 2014. The ENLIL shock connection results shown in the middle panels and the SEPMOD results at the bottom are for an observer located at Venus. The red line in the middle (R_{conn}) panel is drawn at 0.73 AU.

3.3.3. Diagnosis of Ground Level Events

As mentioned earlier, January 2014 included one of the very few GLE events of the solar cycle 24 maximum [e.g., *Gopalswamy et al., 2015*]. The event, early on 6 January, was weak by GLE standards, but notable because of the rarity of cycle 24 GLEs [*Thakur et al., 2014*]. Ground level events are of special interest because they represent a subset of promptly arriving SEP events with an especially energetic component. They are often associated with major flares and fast CME eruptions near the western limb of the Sun’s disk. While there has been discussion regarding a possible flare contribution to the GLE particles, the consensus in the literature seems to be that a relatively low coronal shock source located at $\sim 2\text{--}10 R_s$ is magnetically connected to the Earth’s location when they occur. In addition to the observations suggesting that fast CMEs drive their strongest shocks at early times in their evolution, the Parker spiral field connects Earth’s location to the vicinity of the shock leading edge, or nose—its strongest part—in these near-west limb events. Although ENLIL’s inner boundary is at $21.5 R_s$, above the inferred injection radius, the field geometry upstream of the low coronal shock is nominally radial close to the Sun—at least in the absence of preceding disturbances. This makes it useful to apply ENLIL and SEPMOD toward understanding both the context of the source region as well as the conditions at the shock in its early stages of propagation.

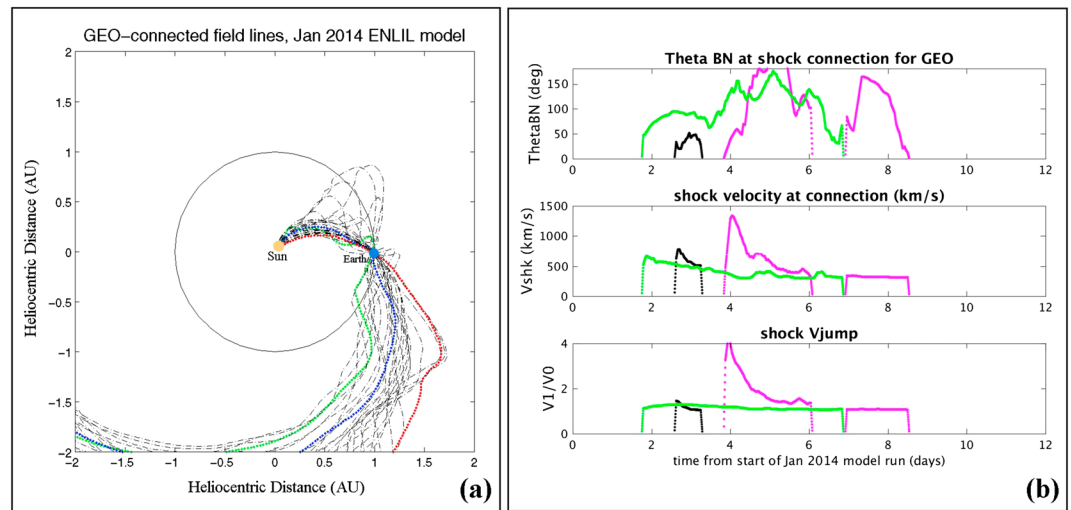


Figure 10. (a) The Earth (GEO)-connected interplanetary field lines plotted in this ecliptic plane view are sampled throughout the ENLIL run (Figure 1e) for the January 2014 study period described earlier. The Earth, whose nominal orbit at 1 AU is the circle, remains in a fixed three o'clock position in this plot. A few of the field lines for times evenly distributed throughout the ENLIL run are colored red, blue, and green, in time sequence (with red at ~10 h from the start, green about 4 days in, and blue at about 8 days in). The field lines are connected to the western heliospheric quadrant as seen from the Earth, as found for most GLEs. The field line distortions are related to the ENLIL ICME(s) that produce SEPs on these field lines. (b) The time series of some of the Earth-connected shock parameters from the ENLIL run for this case, including (from top to bottom) the shock normal angle (theta-BN), the shock speed, and the velocity jump at the shock. Note the time axis is from the start of the ENLIL run on 4 January. The black lines describe the shock most likely associated with the weak GLE on 6 January. Whether the earlier ICME (green) played a role in enabling the GLE shock is unclear. The later, stronger shock connections to another ICME shock (magenta) produced a second, generally stronger, SEP event.

Figure 10a shows a sequence of Earth-connected heliospheric field lines associated with the ENLIL run for this period, which for the Earth included connections to three different ICME shocks (see Figure 1e, middle panel). These provide an idea of the distortions of the fields that occur in connection with the propagation of the shocks, including the presumed GLE-related shock. Figure 10b to the right shows the Earth-connected ENLIL shock characteristics. As seen in the middle and lower panels, the presumed GLE shock initiated late on 5 January (black trace) does not have the strongest shock jump or highest shock speed. The shock normal angle (theta-BN) at the Earth observer connection (top panel) evolves from quasiparallel (theta-BN < 45°), to more quasiperpendicular (thetaBN > 45°), and back to quasiparallel. As seen in Figure 6a, the SEPMOD protons that arrive within minutes of this shock connection decline from their initial intensity peak over more than a day. According to the ENLIL shock connection results in the middle panel of Figure 6a, its local effect on the overall SEP fluxes waned several days later when a stronger shock connection (magenta trace in Figure 10b) started making larger contributions to the proton flux. The models in this case suggest that the duration of the GLE event may have been cut off by observer magnetic disconnection from the shock close to the Sun.

It is notable that even though the ENLIL and SEPMOD results do not include the shock portion inside of 21.5 R_{\odot} , the time history of the observed SEP fluxes at GOES are fairly well represented (Figure 6a). However, the Earth observer observations in Figure 6a as well as the ENLIL results in Figure 10b raise the question of why the 6 January event was a GLE and the subsequent, apparently more intense 8 January event was not. The latter is also inferred to have started with a near-Sun shock connection. The possibility that the coronal shock produced a particularly energetic (>100 MeV) contribution to the 6 January event but not the 8 January event cannot be dismissed, although there may also be an issue of the proton access to the ground [e.g., *Mishev et al., 2014*]. Someday, the coronal portion of the CME/ICME shock formation will be routinely modeled [e.g., see *Kozarev et al., 2013*], at which time SEPMOD can simply extend its range of application inward. In the meantime, the present models can be applied to better understand both the GLE-related shock connection geometry and the influences of other events that may be occurring in the background.

4. Concluding Remarks

In the preceding pages, an updated version of the SEPMOD approach to SEP event modeling at 1 AU was demonstrated using a half dozen periods of multipoint SEP observations and ENLIL models. The results suggest the following:

1. The SEPMOD assumptions of moving, evolving ICME shock sources of SEPs and parallel scatter-free transport provide a viable first-order approximation of SEP event physics, useful for data interpretation and forecasting tool.
2. ENLIL with cone model-initiated ICME shocks based on coronagraph observations makes sufficiently realistic simulations for use with such a tool, when multiple, globally distributed CME events are included and sufficiently long periods (~weeks) and larger heliospheric volumes (to ~5 AU) are modeled.
3. SEPMOD can be applied to understand SEPs and SEP-related phenomena at other inner heliospheric locations (including Mars).

The capability described here can be routinely applied today as long as ENLIL runs with the required shock and observer field line output files are available. Moreover, the current SEPMOD assumptions can be easily manipulated to experiment with changes to those assumptions and to analyze their effects on the outcome. A wide range of changes is possible, including the assumed shock source description and the assumption of scatter-free SEP motion outside of the shock source. This could in principle be part of a larger validation activity, as the examples shown here are based on the original formulation [Luhmann *et al.*, 2007, 2010]. However, a challenge to any potential user is that SEPMOD's results are so dependent on ENLIL producing good simulations of the heliospheric conditions, including the shocks. ENLIL in turn depends on the accuracy of the cone model CME injections, which are subject to the availability of multiperspective imaging for use in triangulating direction and speed. For example, without STEREO coronagraph images, one must work with more ambiguous cone CME initiations, especially in cases of halo events. Indeed, for the March 2015 case discussed above, only one perspective was available for fitting all of the CMEs—introducing greater uncertainty. In general, if multiple CMEs are present, which is often the case, the situation is compounded. In addition, if real-time images are used for the CME parameters, they are often not fully corrected for imaging issues like backgrounds, making quick-turnaround cone model parameter derivations error-prone. Also, as noted earlier, the $21.5 R_s$ inner boundary of ENLIL represents a limit regarding inclusion of coronal portions of the shocks. Thus, anyone applying this or similar methods must always take underlying factors into account in evaluating and applying the results.

It is also necessary to remember that the approach SEPMOD uses was in part motivated by the desire for a relatively simple tool with low computational demands and rapid turnaround. SEPMOD does not include self-consistent treatments of the shock acceleration processes, although it can accommodate different descriptions of the shock source within limits. For example, a different source output could be used for quasi-perpendicular and quasiparallel shocks and a theta-BN dependent enhancement for the ESP enhancement. In general, the basic concepts of a moving, evolving source and source connection geometry that are the basis for SEPMOD can be included more precisely in a number of ways. The current assumption of injection from the shock source only at the time of observer connection emphasizes the shock properties at that time, even though the particles are all followed on the field line until they exit the ENLIL volume (typically up to tens of minutes from their injection). A more accurate approach would involve calculating the complete SEP time profiles on all the field lines that ever connect to the observer and then retroactively constructing the observed time profile from those. This would require considerable increases in computational requirements but would be straightforward. Indeed, SEPMOD should be regarded as an initial version of a numerical experiment, whose assumptions are being tested by comparisons with observations. The results shown here suggest that, at least for an inner heliosphere event analysis and forecast tool, these might be acceptable depending on the user's goals.

The potential investigative and educational aspects of the SEPMOD approach are also worth mentioning. The underlying concepts are relatively straightforward, containing many basic elements of SEP event physics such as the presumption of a 3D, spatially and temporally evolving shock source and continuous particle transport along magnetic fields to an observer—all in a geometrically realistic heliospheric setting. As demonstrated here with several examples, this allows a user to interpret a variety of related data sets and explore their consequences. For example, SEP anisotropies can be derived from SEPMOD results and

applied to event data analyses. In addition, should a coronal shock extension of the heliospheric model become available, inner portions of the observer field line and shock connections can be easily incorporated. And the introduction of coronal ejecta fields would not require any changes in SEPMOD. Finally, the construction of SEPMOD allows it to be used in educational as well as instructional forecasting environments with little investment. Given that the results shown here are completely “hands-off,” with the only case-specific investments made in the form of improvement of ENLIL results, SEPMOD is ready to use.

Acknowledgments

The authors are grateful to the staff of the CCMC for their contributions to deriving the ENLIL cone model parameters, to the SOHO LASCO and STEREO SECCHI investigators for the coronagraph images used, to the GONG Observatory for providing the magnetic synoptic maps used for the ambient solar wind description, to the ACE and STEREO plasma investigation teams for providing 1 AU ENLIL validation data shown here, to the ACE EPAM and GOES EPS Instrument and data providers, and to the MAVEN and Venus Express projects for providing data for the planetary site SEP event model comparisons. This work was supported in part by NASA grant NNX15AG09G to the University of California, Berkeley for the STEREO-IMPACT investigation and by NASA grant NNX15AU01G to the University of New Hampshire for the STEREO PLASTIC investigation. The model development at UC Berkeley is sponsored by the NSF Award 1322826 through the Living With a Star Program in cooperation with NASA. M.L.M., H.B., and Y.L. acknowledge the support of NASA LWS grant NNX15AB80G. WSA-ENLIL+Cone simulation results have been provided by the Community Coordinated Modeling Center at the Goddard Space Flight Center through their public Runs on Request system (<http://ccmc.gsfc.nasa.gov>; run numbers Leila_Mays_033115_SH_1, Leila_Mays_052715_SH_1, Leila_Mays_122116_SH_1, Leila_Mays_122116_SH_2). The WSA model was developed by N. Arge at AFRL, and the ENLIL Model was developed by D. Odstrcil at GMU. The ACE EPAM data were obtained via the CDAWeb portal of the Space Physics Data Facility at GSFC (<https://spdf.gsfc.nasa.gov>), and the GOES data were obtained from the OMNlweb portal (<https://omniweb.sci.gsfc.nasa.gov/ftpbrowser/>). MAVEN SEP data are available through the Planetary Data System PPI node (<http://pds-ppi.igpp.ucla.edu>). Venus Express ASPERA-4 background data were provided through personal communication, courtesy of Y. Futaana at IRF in Kiruna (futaana@irf.se).

References

- Aran, A., B. Sanahuja, and D. Lario (2006), SOLPENCO: A solar particle engineering code, *Adv. Space Res.*, *37*, 1240–1246.
- Aran, A., D. Lario, B. Sanahuja, R. G. Marsden, M. Dryer, C. D. Fry, and S. M. P. McKenna-Lawlor (2007), Modeling and forecasting solar energetic particle events at Mars: The event on 6 March 1989, *Astron. Astrophys.*, *469*, 1123–1134.
- Arge, C. N., J. G. Luhmann, D. Odstrcil, C. J. Schrijver, and Y. Li (2004), Stream structure and coronal sources of the solar wind during the May 12, 1997 CME, *J. Atmos. Sol. Terr. Phys.*, *66*, 1295–1309.
- Bain, H. M., M. L. Mays, J. G. Luhmann, Y. Li, L. K. Jian, and D. Odstrcil (2016), Shock connectivity in the August 2010 and July 2012 solar energetic particle events inferred from observations and ENLIL modeling, *Astrophys. J.*, *825*, 1, doi:10.3847/0004-637X/825/1/1.
- Barabash, S., et al. (2007), The Analyzer of Space Plasmas and Energetic Atoms (ASPERA-4) for the Venus Express mission, *Planet. Space Sci.*, *55*, 1772–1792.
- Cane, H. V., D. V. Reames, and T. T. Roseninge (1988), The role of interplanetary shocks in the longitude distribution of solar energetic particles, *J. Geophys. Res.*, *93*, 9555–9567.
- Cane, H. V., R. A. Mewaldt, C. M. S. Cohen, and T. T. von Roseninge (2006), Role of flares and shocks in determining solar energetic particle abundances, *J. Geophys. Res.*, *111*, doi:10.1029/2005JA011071.
- Clarke, J. T., et al. (2005), Morphological differences between Saturn’s ultraviolet aurorae and those of Earth and Jupiter, *Nature*, *433*, 717–719.
- Cohen, C. M. S. (2006), Observations of energetic storm particles: An overview, in *Solar Eruptions and Energetic Particles*, *Geophys. Monogr. Ser.*, vol. 165, edited by N. Gopalswamy, R. Mewaldt, and J. Torsti, pp. 275–282, AGU, Washington, D. C.
- Cohen, C. M. S., G. M. Mason, R. A. Mewaldt, and M. E. Weidenbeck (2014), The longitudinal dependence of heavy ion composition in the 2013 April 11 solar energetic particle event, *Astrophys. J.*, *793*, 35, doi:10.1088/0004-637X/793/1/35.
- Desai, M., and J. Giacalone (2016), Large gradual solar energetic particle events, *Living Rev. Sol. Phys.*, *13*, 3, doi:10.1007/s41116-016-0002-5.
- Dewey, R. M., D. N. Baker, M. L. Mays, D. A. Brain, B. M. Jakosky, J. S. Halekas, J. E. P. Connerney, D. Odstrcil, J. G. Luhmann, and C. O. Lee (2016), Continuous solar wind forcing knowledge: Providing continuous conditions at Mars with the WSA-ENLIL+Cone model, *J. Geophys. Res. Space Physics*, *121*, 6207–6222, doi:10.1002/2015JA021941.
- Drury, L. O. (1983), An introduction to the theory of diffusive shock acceleration of energetic particles in tenuous plasmas, *Rep. Prog. Phys.*, *46*, 973–1027.
- Ellison, D. C., F. C. Jones, and S. P. Reynolds (1990), First-order Fermi particle acceleration by relativistic shocks, *Astrophys. J.*, *360*, 702–714.
- Futaana, Y., et al. (2008), Mars Express and Venus Express multi-point observations of geoeffective flare events in December 2006, *Planet. Space Sci.*, *56*, 873–880.
- Gold, R. E., S. M. Krimigis, S. E. Hawkins, D. K. Haggerty, D. A. Lohr, E. Fiore, T. P. Armstrong, G. Holland, and L. J. Lanzerotti (1998), Electron, proton and alpha monitor on the Advanced Composition Explorer spacecraft, *Space Sci. Rev.*, *86*, 541–562.
- Gopalswamy, N., P. Mäkelä, S. Yashiro, H. Xie, S. Akiyama, and N. Thakur (2015), High energy solar particle events in cycle 24, *J. Phys. Conf. Ser.*, *642*, 1–9.
- Gray, C. L., N. J. Chanover, T. G. Slinger, and K. Molaverdikhani (2014), The effect of solar flares, coronal mass ejections, and solar wind streams on Venus’ 5577 Angstrom oxygen green line, *Icarus*, *233*, 342–347.
- Hassler, D., et al. (2014), Mars surface radiation environment measured with the Mars Science Laboratory’s Curiosity rover, *Science*, *343*(6169), 1244797, doi:10.1126/science.1244797.
- Heras, A. M., B. Sanahuja, Z. K. Smith, T. Detman, and M. Dryer (1992), The influence of the large-scale interplanetary shock structure on a low energy particle event, *Astrophys. J.*, *391*, 359–369.
- Heras, A. M., B. Sanahuja, T. R. Sanderson, R. G. Marsden, and K. P. Wenzel (1994), Observational signatures of the influence of the interplanetary shocks on the associated low-energy particle events, *J. Geophys. Res.*, *99*, 43–51.
- Jakosky, B. M., et al. (2015), MAVEN observations of the response of Mars to an interplanetary coronal mass ejection from the Sun, *Science*, *350*(6261), aad0210, doi:10.1126/science.aad0210.
- Jones F. C., and D. C. Ellison (1991), The plasma physics of shock acceleration, *Space Sci. Rev.*, *58*, 259–346.
- Kallenrode, M.-B., and G. Wibberenz (1997), Propagation of particles injected from interplanetary shocks: Black box model and its consequences for acceleration theory and data interpretation, *J. Geophys. Res.*, *102*, 22,311–22,334.
- Kallenrode, M. B. (2003), Current views on impulsive and gradual solar energetic particle events, *J. Phys. G Nucl. Part Phys.*, *29*, 965–981.
- Kozarev, K., R. M. Evans, N. A. Schwadron, M. A. Dayeh, K. E. Opher, K. E. Korreck, and B. van der Holst (2013), Global numerical modeling of energetic proton acceleration in a coronal mass ejection traveling through the solar corona, *Astrophys. J.*, *778*, 1–13.
- Klecker, B., et al. (2006), Energetic particle observations, *Space Sci. Rev.*, *123*, 217–250.
- Kocharov, L., V. J. Pizzo, D. Odstrcil, and R. D. Zwickl (2009), A unified model of solar energetic particle transport in structured solar wind, *J. Geophys. Res.*, *114*, A05102, doi:10.1029/2008JA013837.
- Kota, J., W. B. Manchester, J. R. Jokipii, D. L. DeZeeuw, and T. I. Gombosi (2005), Simulations of SEP acceleration and transport at CME-driven shocks, in *The Physics of Collisionless Shocks*, *AIP Conference Proceedings*, vol. 781, pp. 201–206.
- Lario, D., B. Sanahuja, and A. M. Heras (1997), Modeling the interplanetary propagation of 0.1–20 MeV shock accelerated protons II: Energy spectrum and evolution of the injection rate, *Adv. Space Res.*, *20*, 121–126.
- Lario, D., B. Sanahuja, and A. M. Heras (1998), Energetic particle events: Efficiency of interplanetary shocks as 50 keV E E E 100 MeV proton accelerators, *Astrophys. J.*, *509*, 415–434.
- Lario, D., N. E. Raouafi, R.-Y. Kwon, J. Zhang, R. Gomez-Herrero, N. Dresing, and P. Riley (2014), The solar energetic particle event on 2013 April 11: An investigation of its solar origin and longitudinal spread, *Astrophys. J.*, *797*, 8, doi:10.1088/0004-637X/797/1/8.
- Larson, D. E., et al. (2015), The MAVEN solar energetic particle investigation, *Space Sci. Rev.*, *195*, 153–172.

- Lee, C. O., C. N. Arge, D. Odstrcil, G. Millward, V. Pizzo, J. M. Quinn, and C. J. Henney (2013), Ensemble modeling of CME propagation, *Sol. Phys.*, *285*, 349–368.
- Lee, C. O., et al. (2017), MAVEN observations of the solar cycle 24 space weather conditions at Mars, *J. Geophys. Res. Space Physics*, *122*, 2768–2794, doi:10.1002/2016JA023495.
- Li, Gang, G. P. Zank, and W. K. M. Rice (2003), Energetic particle acceleration and transport at coronal mass ejection-driven shocks, *J. Geophys. Res.*, *108*(A2), 1082, doi:10.1029/2002JA009666.
- Liu, Y., et al. (2014), Observations of an extreme storm in interplanetary space caused by successive coronal mass ejections, *Nat. Commun.*, *5*, 3481, doi:10.1038/ncomms4481.
- Luhmann, J. G., S. C. Solomon, J. A. Linker, J. G. Lyon, Z. Mikic, D. Odstrcil, W. Wang, and M. Wiltberger (2004), Coupled model simulation of a Sun-to-Earth space weather event, *J. Atmos. Sol. Terr. Phys.*, *66*(15–16), 1243–1256.
- Luhmann, J. G., S. A. Ledvina, D. Krauss-Varban, D. Odstrcil, and P. Riley (2007), A heliospheric simulation-based approach to SEP source and transport modeling, *Adv. Space Res.*, *40* (3), 295–303.
- Luhmann, J. G., S. A. Ledvina, D. Odstrcil, M. J. Owens, X.-P. Zhao, Y. Liu, and P. Riley (2010), Cone model-based SEP event calculations for applications to multipoint observations, *Adv. Space Res.*, *46*, 1–21.
- Luhmann, J. G., Y. Li, D. J. Bercik, L. Wang, and D. Odstrcil (2012), Issues in heliospheric field mapping to flare SEP sources, in *Space Weather: The Space Radiation Environment, AIP Conference Proceedings*, vol. 1500, pp. 3–13, doi:10.1063/1.4768737.
- Mäkelä, P., N. Gopalswamy, S. Akiyama, H. Xie, and S. Yashiro (2011), Energetic storm particle events in coronal mass ejection-driven shocks, *J. Geophys. Res.*, *116*, A08101, doi: 10.1029/2011JA016683.
- Mays, M. L., et al. (2015a), Ensemble modeling of CMEs using the WSA-ENLIL+cone model, *Sol. Phys.*, *290*, 1775–1814, doi:10.1007/s11207-105-0692-1.
- Mays, M. L., et al. (2015b), Propagation of the 7 January 2014 CME and resulting geomagnetic non-event, *Astrophys. J.*, *812*, 1–15, doi:10.1088/0004-637X/812/2/145.
- Marsh, M. S., S. Dalla, M. Dierckx, T. Laitinen, and N. B. Crosby (2015), SPARX: A modeling system for solar energetic particle radiation space weather forecasting, *Space Weather*, *13*, 386–394, doi:10.1002/2014SW001120.
- Mewaldt, R. A. (2006), Solar energetic particle composition, spectra, and space weather, *Space Sci. Rev.*, *124*, 303–316.
- Mewaldt, R. A., et al. (2008), The Low Energy Telescope (LET) and SEP Central Electronics for the STEREO mission, *Space Sci. Rev.*, *136*, 285–362.
- Mishev, A. L., L. G. Kocharov, and I. G. Usoskin (2014), Analysis of the ground level enhancement on 17 May 2012 using data from the global neutron monitor network, *J. Geophys. Res. Space Physics*, *119*, 670–679, doi:10.1002/2013JA019253.
- Moestl, C., et al. (2015), Strong coronal channeling and interplanetary evolution of a solar storm up to Earth and Mars, *Nat. Commun.*, *6*, 7135, doi:10.1038/ncomms8135.
- Odstrcil, D., and V. J. Pizzo (1999), Distortion of the interplanetary magnetic field by three dimensional propagation of coronal mass ejections in a structures solar wind, *J. Geophys. Res.*, *104*, 28,225–28,239.
- Odstrcil, D., P. Riley, and X. P. Zhao (2004), Numerical simulation of the 12 May 1997 interplanetary event, *J. Geophys. Res.*, *109*, A02116, doi:10.1029/2003JA010135.
- Odstrcil, D., V. J. Pizzo, and C. N. Arge (2005), Propagation of the 12 May 1997 interplanetary coronal mass ejection in evolving solar wind structures, *J. Geophys. Res.*, *110*, A02106, doi:10.1029/2004JA010745.
- Palmer, J. D. (1982), Transport coefficients of low energy cosmic rays in interplanetary space, *Rev. Geophys. Space Phys.*, *20*, 335–351.
- Phillips, J. L., J. G. Luhmann, and A. I. F. Stewart (1986), The Venus ultraviolet aurora, observations at 130.4nm, *Geophys. Res. Lett.*, *13*, 1047–1050.
- Pizzo, V. J. (1991), The evolution of corotating stream fronts near the ecliptic plane in the inner solar system II—Three-dimensional tiled dipole fronts, *J. Geophys. Res.*, *96*, 5405–5420.
- Pomoell, J., A. Aran, C. Jacobs, R. Rodriguez-Gasen, S. Poedts, and B. Sanahuja (2015), Extraction of the characteristics of the MHD shock front at the cobpoint, *J. Space Weather Space Clim.*, *5*, 13, doi:10.1051/swsc/201515.
- Reames, D. V. (1999), Particle acceleration at the Sun and in the Heliosphere, *Space Sci. Rev.*, *90*, 413–491.
- Reames, D. V., C. K. Ng, and A. J. Tylka (2013), Spatial distribution of solar energetic particles in the inner heliosphere, *Sol. Phys.*, *285*, 233–250.
- Richardson, I. G., T. T. von Rosenvinge, H. V. Cane, E. R. Christian, C. M. S. Cohen, A. W. Labrador, R. A. Leske, R. A. Mewaldt, M. E. Wiedenbeck, and E. C. Stone (2014), >25 MeV proton events observed by the high energy telescopes on the STEREO A and B spacecraft and/or at the Earth during the first ~seven years of the STEREO mission, *Sol. Phys.*, *289*, 3059, doi:10.1007/s11207-014-0524-8.
- Rouillard, A., et al. (2011), Interpreting the properties of solar energetic particle events by using combined imaging and modeling of interplanetary shocks, *Astrophys. J.*, *735*, 7–17, doi:10.1088/0004-637X/735/1/7.
- Russell, C. T., et al. (2013), The very unusual interplanetary coronal mass ejection of 2012 July 23: A blast wave mediated by solar energetic particles, *Astrophys. J.*, *770*, 38, doi:10.1088/0004-637X/770/1/38.
- Schwadron, N., et al. (2010), Earth-Moon-Mars radiation environment module framework, *Space Weather*, *8*, S00E02, doi:10.1029/2009SW000523.
- Schneider, N. M., et al. (2015), Discovery of diffuse aurora on Mars, *Science*, *350*(6261), aad0313, doi:10.1126/science.aad0313.
- Schrijver, C. J., et al. (2015), Understanding space weather to shield society: A global road map for 2015–2025 commissioned by COSPAR and ILWS, *Adv. Space Res.*, *55*, 2745–2807.
- Taktakishvili, A., M. Kuznetsova, P. MacNeice, M. Hesse, L. Rastaetter, A. Pulkkinen, A. Chulaki, and D. Odstrcil (2009), Validation of the coronal mass ejection predictions at the Earth orbit estimated by ENLIL heliospheric cone model, *Space Weather*, *7*, S03004, doi:10.1029/2008SW000448.
- Thakur, N., N. Gopalswamy, H. Xie, P. Makela, S. Yashiro, S. Akiyama, and J. M. Davila (2014), Ground level enhancement in the 2014 January 6 solar energetic particle event, *Astrophys. J. Lett.*, *790*, L13, doi:10.1088/2041-8205/790/1/L13.
- Tylka, A. J., and M. A. Lee (2006), A model for spectral and compositional variability at high energies in large, gradual solar particle events, *Astrophys. J.*, *646*, 1319–1334.
- von Rosenvinge, T. T., et al. (2008), The high energy telescope for STEREO, *Space Sci. Rev.*, *136*, 391–436.